OBSERVATIONS OF THE SPATIAL DISTRIBUTION OF BUBBLES GENERATED BY BREAKING WAVES

by

GREGORY BLAIR CRAWFORD

B.Sc., University of Victoria, 1983

A THESIS SUBMITTED IN PARTIAL FULFILLMENT
OF THE REQUIREMENTS FOR THE DEGREE OF
MASTER OF SCIENCE
in the Department of Physics

We accept this thesis as conforming to the required standard

[redacted]
D.M. Farmer

[redacted]
J.T. Weaver

[redacted]
H.W. Dosso

[redacted]
P. van den Driessche

[redacted]
N.R. Chapman

UNIVERSITY OF VICTORIA

SEPTEMBER 1985

Supervisors: Dr. D.M. Farmer and Dr. J.T. Weaver

Abstract

This thesis represents a study of the spatial distribution of sub-surface bubbles generated by breaking wind waves. Observations of bubbles were obtained using an upward-pointing acoustic transducer mounted on a submarine. Experiments were carried out about 10km off the coast of Monterey, California at wind speeds of about $3ms^{-1}$ to $11ms^{-1}$.

For the first time, estimates of the concentration of bubbles, N, have been determined from acoustic backscatter levels. The measurements are also unique in that they represent two-dimensional profiles of N, indicating both vertical and horizontal dependence. At low wind speeds, few identifiable patches of bubbles were observed. At higher wind speeds, the concentration of bubbles was observed to increase. In addition, the depths to which bubbles penetrate increased with wind speed.

Mean vertical profiles of N indicated an exponential dependence on depth, which is consistent with a simple one-dimensional diffusion model. The mean bubble concentration at the surface, N_o, was found to increase with wind speed U_{10} as $N_o \sim U_{10}^{(3.0\pm0.3)}$. Estimates of the e-folding scale, z_e, increased in

general with wind speed, but the level of convective turbulence also influenced the values of z_e. The bubble plumes were found to be more columnar when the air-sea temperature difference was more negative (i.e. when the level of convective turbulence was greater).

Ratios of the horizontal extents of bubble plumes, as measured at different angles to the wind direction, were found to be consistent with the ratio of the horizontal scales over which waves break on the ocean surface. A data set collected while travelling in the downwind direction was found to have a spectral peak corresponding to a separation of 45m between bubble plumes, consistent with the expected spacing between breaking events on the surface. These results provide evidence that the bubble plumes are directly related to breaking waves on the ocean surface.

[redacted]

D.M. Farmer

[redacted]

J.T. Weaver

[redacted]

H.W. Dosso

[redacted]

P. van den Driessche

[redacted]

N.R. Chapman

Table of Contents

List of Tables

List of Figures

Acknowledgements

I would very much like to thank my supervisors Dr. D.M. Farmer and Dr. J.T. Weaver for their valuable assistance and guidance during the course of this research. I would also like to thank Dr. T.R. Osborn for providing an opportunity to make the observations described in this thesis.

This work could not have been done without the use of the facilities of the Institute of Ocean Sciences (Patricia Bay) and the assistance of several of its scientists and support staff. In particular, I would like to acknowledge Dr. A.F. Bennett, Dr. A.D. Booth, Dr. A. Gargett, George Chase, Jim Galloway, Grace Kamitakahara-King and Ron Teichrob.

Thanks are due to my fellow graduate students Richard Dewey, Ben Huber, Del Huston, Svein Vagle and Len Zedel for their constructive comments and criticisms. Additional thanks are due to Dr. T. Stanton and Dr. L. Haury for providing me with additional data under duress.

Financial support for this project was provided through the Department of Fisheries and Oceans and the U.S. Office of Naval Research. Graduate student support was provided by N.S.E.R.C., the

Science Council of B.C. (through a G.R.E.A.T. award) and the R.M. Pearce Memorial Fellowship. This support is gratefully acknowledged.

Dedication

To my parents, with much love

Chapter 1

Introduction

When ocean waves break, they inject air bubbles into the near-surface ocean in significant quantities. The larger bubbles, being very buoyant, return to the surface relatively quickly. Smaller bubbles, on the other hand, are much less buoyant and hence act like passive contaminants in the ocean. The distribution of small bubbles is therefore intimately related to the local fluid dynamics. Bubbles generated by breaking waves are also known to be involved in a number of important oceanographic processes, including: droplet ejection (Blanchard and Woodcock 1957); gas exchange (Kanwisher 1963; Memery and Merlivat 1984; Thorpe 1984a); electrical charge exchanges (Blanchard 1963); the formation of organic particles (Sutcliffe et al 1963); bacteria transport (Blanchard and Syzdik 1972, 1974); chemical fractionation (Duce and Hoffman 1976); propagation of underwater sound (Medwin 1974).

In October 1984, a number of acoustic experiments were carried out off the coast of Monterey, California on board the submarine USS DOLPHIN. In particular, acoustic observations of bubbles located near the ocean surface were obtained using a 119kHz, upward-pointing echo-sounder. This thesis describes those observations in terms of the horizontal and vertical distribution of bubbles. Before

discussing the bubbles further, however, we first present a brief review of relevant air-sea interactions in order to provide some necessary background for the reader.

1.1 Summary of Oceanic Response to Wind Forcing

Neither the ocean nor the atmosphere are truly isolated dynamical systems. The interactions between the two fluids control the exchange of energy, momentum, heat and gas across the interface. Air-sea interaction has been a field of investigation for many years, but our understanding of the processes involved is still severely limited. This is due in part to the complexity of these processes and in part to the environmental constraints associated with their study. Nevertheless, the study of the processes governing air-sea interactions is of great importance in our understanding of both the atmosphere and the ocean.

When the wind blows across the surface, it transfers energy and momentum to the ocean. This transfer takes place through a number of processes. The most familiar of such processes is the generation of waves. Such waves are called, appropriately enough, wind waves (see Kinsman 1965) and are a form of surface gravity wave.

In light winds, the waves generated are quite small (with wavelengths of the order of a few centimeters). As the strength of the wind increases, the waves grow higher and longer. Wave growth, however, is subject to a limiting process associated with the steepness of the waves (i.e. the ratio of wave height to wavelength). Once the steepness of a wave increases beyond some critical value, the wave breaks.

If the wind remains steady for a sufficient period of time, the ocean surface will reach an equilibrium state called a 'fully-developed sea', in which the input of energy provided by the wind is balanced by the loss of energy in the waves due to wave-breaking. Three factors have been associated with the size of wind waves and the point at which the sea becomes fully-developed: the wind force, or equivalently the wind speed; the fetch, or uninterrupted distance over which the wind blows at a fixed velocity; the duration over which the wind blows at a fixed velocity. Generally, higher wind speeds and longer fetches generate higher and longer waves and require longer durations before an equilibrium state is reached.

Locally-forced waves are referred to as sea, while waves which have escaped the influence of the generating wind are called swell. Waves associated with sea are of higher frequency than those

associated with swell (Kinsman [1965] suggests that a 'rule of thumb' for distinguishing between sea and swell is to presume a transition occurs at 0.1Hz, but acknowledges that one must allow for much overlap). Wave shapes associated with swell are nearly sinusoidal, while waves associated with sea are typically trochoidal in shape. Sea also tends to be steeper, more rugged and more confused (random) than swell.

The dispersion relation for surface gravity waves is given by

$$c^2 = \frac{g}{k} \tanh(kH) \qquad (1.1)$$

where $k=2\pi/\lambda$ is the wavenumber of the wave, λ is its wavelength, c is its phase speed, g is gravitational acceleration and H is the total water depth (c.f. Lamb, 1932). For water which is much deeper than half the wavelength, the phase velocity is approximately

$$c = (g/k)^{1/2} . \qquad (1.2)$$

Longer waves are seen to travel faster than shorter waves. They escape the region of wave generation to form swell. Dissipation of swell takes place slowly through the effects of molecular viscosity as the waves continue to propagate.

Much research effort has been spent on wave analysis and prediction. Since the wave field is random, much of the work has been based on the evaluation of a few fundamental statistical

quantities, such as the significant wave height $H_{1/3}$. This is defined as the average height of the 1/3 highest waves, as measured from crest to trough. Empirically-derived curves have been developed to predict $H_{1/3}$ and the associated wave period, $T_{1/3}$, under fetch-limited and duration-limited conditions (e.g. U.S. Army Coastal Engineering Research Center 1984).

With the advent of sophisticated wave-measuring devices, attention has been focussed on evaluation and modelling of the wave spectrum, that is the power spectrum of the wave height at a given location. This represents a more modern approach to the description of the wave field, relating the sea state to a spectrum of wave energies and periods rather than to discrete statistical quantities (Thomson 1981). Waves, however, do not extend out to infinity, but instead occur in localized groups. The wave groups are limited in extent because the event which generated them is limited in extent and duration.

Under calm conditions, the wave spectrum is nearly flat. In a fully-developed sea, a well-defined peak appears in the spectrum, which tapers off at higher frequencies. The presence of swell can also introduce a large peak in the spectrum, although at a lower frequency than the dominant frequency asociated with the locally-forced waves.

Wave-breaking is a complicated nonlinear effect. The most common type of breaking wave observed in deep water is the 'spilling breaker'. This is identified as a steep wave which has a turbulent plume of frothy water running down its forward face (Cokelet 1977). The plume is recognized as a 'whitecap' or 'whitehorse'. The wind can also cause a wave to break directly by blowing off the top of the wave.

Breaking waves entrain air bubbles and hence are responsible for an increase in gas flux across the air-sea interface. They also transfer momentum and energy across the surface through the generation of turbulence. Laboratory measurements by Donelan (1978) have indicated, however, that the turbulence associated with breaking waves is limited to within a depth below the surface of the order of the wave height.

For the most part, the initial response of the ocean surface to wind forcing is through wave generation, growth and breaking. The fluid particles themselves move in nearly-circular orbits in response to the wave action. However, the wind also generates a net lateral motion of the surface layer of fluid, thereby creating a shear flow in the uppermost part of the ocean. Under suitable conditions, turbulence will arise from the shear flow due to flow instabilities (Tennekes and Lumley 1972).

Turbulence can also be produced by convection, the presence of which is dependent on the net heat flux across the air-sea interface. The net heat flux is comprised of three main components: the sensible heat flux, which is identified with the direct heat conduction across the interface (i.e. due to the presence of an air-sea temperature difference ΔT); the evaporative heat flux, due to cooling by evaporation; the back-radiative heat flux, due to the absorption and re-emission of solar radiation (Gill 1982). If the net heat flux is upwards, then fluid particles just below the surface lose heat to the atmosphere and their density increases. These particles are then heavier than their surroundings and therefore sink, to be replaced by the warmer water just below. This flow is identified as convective turbulence.

Field observations of upper ocean turbulence are very limited (see Dillon and Caldwell 1980; Oakey 1982; Shay and Gregg 1984). However, it is generally assumed that turbulence, generated by convection and indirectly by the wind, is responsible for the downward diffusion of energy, momentum and gas (the latter through bubble transportation), as well as the mixing of the upper ocean and subsequent deepening of the thermocline.

Another type of flow which occurs in the upper ocean in the presence of wind is called Langmuir circulation. This flow takes the form of alternating right-handed and left-handed vortices whose axes

are aligned with the wind. They can frequently be identified by the presence of long, narrow streaks on the surface, called 'wind rows'. The streaks result from the collection of floating substances (e.g. marine organisms, foam from breaking waves, seaweed) in the regions of flow convergence at the surface. The spacing between wind rows indicates the separation between pairs of vortices (or Langmuir cells).

Since the initial study of this phenomenon by Langmuir (1938), several observations of wind rows and Langmuir circulations have been obtained in lakes and in the ocean. Much variation in wind row separation has been found, but in the ocean the spacing generally falls between about 5m and 50m (for a recent review of theories and observations of Langmuir circulation, see Leobovich[1983]).

Numerous theories on the mechanism of generation of the flow have been put forward and subsequently cast aside over the years. The most prominent theories today suggest that the flow is produced by complicated interactions between the current field and the wave field, both of which are functions of the wind conditions (c.f. Garrett 1976; Craik and Leobovich 1976; Craik 1977). Support for this concept has been garnered by a number of laboratory studies (c.f. Faller and Perini 1984), which have produced flows resembling Langmuir circulation only when both waves and a shear flow are present. It is still not known, however, how much of a role Langmuir

circulation plays in the dynamics of the upper ocean.

1.2 Review of Previous Bubble Studies

Most of the pioneering work on the distribution of ocean bubbles has been performed using bubble traps. A bubble trap is basically a box or tube structure with a transparent observing plate. The trap is operated by immersing it in water, obtaining a water sample and then orienting the trap so the transparent side is on top. Bubbles within the water sample are free to rise and accumulate against the underside of the clear face. After sufficient time has passed for the bubbles to traverse the length of the trap, the bubbles under the observing plate are measured and counted.

Using their bubble trap, Blanchard and Woodcock (1957) found that the bubble density increases rapidly with windspeed. Glotov et al (1962) found similar results using a bubble trap in a wind-wave tank. Kolovayev (1976) used a bubble trap and camera system (which photographed the observing plate) to determine oceanic bubble populations in the deep ocean.

Concern has been expressed in the literature (e.g. Blanchard

and Woodcock 1957) about measurements of bubbles with small radii (of the order of 10μm and less) using bubble traps. Many of these small bubbles will dissolve into the water sample before they can traverse the length of the trap and reach the observing plate. Consequently, methods for direct observations have been developed. Medwin (1970) made direct photographic observations of bubbles near shore. More recently, Johnson and Cooke (1979) used a camera system suspended from a freely-drifting float to make oceanic bubble observations.

Medwin (1970, 1977a) has evaluated bubble populations acoustically by measuring their scattering and absorption properties as a function of frequency. In addition, he and his co-workers have made estimates of bubble fraction (the relative volume of bubble gas to liquid) by analyzing phase and amplitude fluctuations of sound passing through bubbles near the ocean surface (Medwin 1974; Medwin et al 1975).

Wu (1981) has reviewed and summarized the results of Johnson and Cooke (1979), Kolovayev (1976) and Medwin (1970). Of particular interest is the bubble distribution (also referred to as the bubble spectrum) n(a), where n is the number of bubbles per unit volume with a given bubble radius a. The spectra obtained from Johnson and Cooke's data are quite similar to those based on Kolovayev's results. Both sets of spectra indicate that n(a) varies as $n(a) \sim a^{-m}$ down to a radius of about 50 μm, where m=5 from Johnson and Cooke's

data and m=3.5 from that of Kolovayev. The spectra appear to peak at around 40-50μm and then fall off with decreasing radius. In addition, the number of bubbles varies approximately exponentially with depth. Wu (1981) noted that these results suggest there may be an equilibrium spectral distribution for n(a).

Medwin's (1970, 1977a) acoustic observations show somewhat different characteristics, including much larger bubble populations than observed by Johnson and Cooke or Kolovayev at the same depths and under similar wind conditions. His first study (Medwin 1970), performed in coastal waters and in light winds (about $2ms^{-1}$) indicated that the bubble spectrum varies with bubble radius as approximately $n \sim a^{-4}$ for large bubbles ($a > 80\mu m$) and as $n \sim a^{-2}$ for small bubbles ($a < 80\ \mu m$). He also determined that the number of bubbles with radii less than 60μm varies with depth below the sea surface z (in meters) as $n \sim \exp(-z/7)$, while the number of bubbles with radii equal to or greater than 60μm follows a power law $n \sim z^{-0.5}$.

In the later study, Medwin (1977a) made a more detailed bubble survey, predominantly in Monterey Bay, under a variety of wind conditions. Similar results were obtained for the spectral variation with radius as for the previous study, but the dependence of bubble populations on depth was less straightforward. In fact, for data collected at a wind speed of about 4 ms^{-1}, he observed more bubbles

near the bottom of the bay than near the surface. Dalen and Lovik (1981) have also found very large estimates of bubble population using transducers mounted on the hull of a ship. They estimated bubble populations by studying separately the volume reverberation from bubbles in the ocean and variations in the attenuation of sound scattered back from the sea floor.

It has generally been presumed in the literature that the dominant production process for bubbles observed by Johnson and Cooke (1979) and Kolovayev (1976) was entrainment of air by breaking waves, while some other process (such as biological bubble production) was responsible for the observations of Medwin (1970, 1977a) and Dalen and Lovik (1981). Consequently, these latter results have been for the most part disregarded in recent studies of bubbles generated by wave-breaking.

Laboratory studies of bubble size spectra have recently been made by Hsu et al (1984) and Broecker and Siems (1984). They have observed peaks in the bubble distribution at a radius of between 40 and 50μm (presumably there is an error in the plot of bubble spectra in Hsu et al [1984] - the label on the bubble size axis would appear to be too large by a factor of ten). Both studies found the power-law dependence of the distribution was a function of depth, with the value of m increasing with depth. Little dependence of the bubble spectra on wind speed was observed.

Aleksandrov and Vaindruk (1974) used an upward-pointing transducer mounted on the sea floor at 20m depth and 1km offshore. They studied acoustically the thickness of the bubble layer and found that it varied on two time scales. The oscillations of shorter period were associated with orbital motions of the ocean in the presence of surface waves. They attributed the longer time scale variations to turbulent motions in the upper ocean.

Thorpe and his co-workers have made several studies of near-surface bubbles in lakes and ocean using acoustic systems. Observations by Thorpe and Stubbs (1979) suggested the shape of bubble clouds is dependent on the sign of the air-sea temperature gradient, which indicates the direction of heat flux across the interface. When the air was colder than the water (a condition which can set up convection in the upper ocean), the clouds appeared to be more columnar in shape; when the water was colder than the air (a condition of stability), the clouds appeared more 'billow-like'. Thorpe and Humphries (1980) obtained evidence that the clouds of bubbles are generated by breaking waves.

Thorpe (1982) studied variations in bubble populations based on the levels of acoustic backscatter. Reasonable agreement was obtained between mean observed backscatter levels and theoretical levels (based on the data of Johnson and Cooke [1979]) under similar

wind conditions. He also found stronger backscatter levels in the ocean than in a lake under similar atmospheric conditions.

Thorpe et al (1982) and Thorpe and Hall (1983) have used bottom-mounted side-scan sonar systems to study near-surface waters in a lake and in the ocean, respectively. These instruments were aligned so as to obtain horizontal profiles of acoustic targets near the surface. The authors were able to observe characteristics of bubble clouds, near-surface currents, internal waves and breaking surface waves. In particular, Thorpe and Hall (1983) compared bubble clouds under different wind conditions. At low wind speeds (up to about 6 ms^{-1}), wave breaking was rare and brief, and the bubble clouds were few and distinct. At higher wind speeds, waves broke more frequently and for longer periods of time. In these latter cases, a layer of bubbles was observed to form beneath the ocean surface, punctuated by 'plumes' of bubbles recently entrained by the breaking waves.

Other acoustic techniques have been employed in the study of bubbles. Recently, Farmer and Lemon (1984) made estimates of the population density of bubbles based on the attenuation of wind-generated sound by bubbles below the sea surface. In addition, a high-resolution technique for measuring bubble size using non-linear mixing of two frequencies has been developed and tested in the laboratory (Newhouse and Shankar 1984; Chapelon et al 1985).

A variety of dynamical models of bubble transport have been developed which help to explain observed bubble distributions or suggest different distributions. Garrettson (1973) developed a very general statistical equation for bubble transport. This work provided the basis for a simple turbulent diffusion model obtained by Crowther (1980), who neglected the effects of bubble acceleration and changes in bubble radii due to hydrostatic pressure and gas diffusion. Kerman (1982) has developed a turbulent diffusion model based on the mass of bubbles produced at the surface.

Thorpe (1982, 1984b,c) has created models of bubble transport, based on Garrettson's work, which include the effects of pressure and of gas diffusion. Thorpe (1984d) has also modelled bubble dynamics and distributions in the presence of a flow resembling Langmuir circulation and has shown this flow produces horizontal variations in the sub-surface bubble distribution.

Crowther (1985) has proposed a new bubble distribution function, which is similar to his previous model (Crowther 1980) for larger bubbles and is supposedly consistent with the results obtained by Johnson and Cooke (1979) and Thorpe (1982) for smaller bubbles.

Most of the models mentioned here are based on simple functional forms of turbulence and of flow. Kitaigorodskii (1984) has indicated that the transfer of gas across the air-sea interface

is governed primarily by 'patchy' turbulence generated by breaking wind waves. As noted previously, however, few measurements of turbulence in the upper ocean have been made to support or disclaim this theory.

1.3 Summary of Work Done in this Thesis

The purpose of the research discussed in this thesis was to study the spatial distribution of sub-surface bubbles generated by breaking waves. We have participated in a number of experiments which were carried out near Monterey, California during October 1984. Observations of bubbles were obtained using an upward-pointing acoustic transducer mounted on the deck of the submarine USS DOLPHIN.

We present here for the first time estimates of the concentration of bubbles evaluated from acoustic backscatter levels. The results are also unique in that both the vertical and horizontal variability of the concentration of bubbles are provided.

Observations of the spatial distribution of bubbles under conditions of light winds ($3ms^{-1}$) and moderate winds ($8\text{-}11ms^{-1}$) are discussed. Profiles of the mean concentration of bubbles at

different wind speeds are provided and indicate an exponential dependence with depth. Estimates of the bubble concentration at the surface N_o indicate a dependence on the wind speed U_{10}(measured at 10m above the surface) of the form $N_o \sim U_{10}^{3.0\pm0.3}$. The e-folding depth z_e (i.e. the increase in depth required for the mean bubble concentration to decrease by a factor of e^{-1}) was found to increase in general with increasing wind speed; but there was indication that the level of convective turbulence can also influence the e-folding depth. The bubble plumes were found to be more columnar in shape in the presence of more negative air-sea temperature difference (suggesting a greater level of convective turbulence).

Ratios of horizontal extents of the bubble plumes, as measured at different angles to the wind direction, were found to be consistent with the ratio of the horizontal scales over which waves break. In addition, a data set collected while travelling in the downwind direction was found to have a spectral peak corresponding to a separation of 45m between bubble plumes, consistent with the expected spacing between breaking events on the surface. These results provide evidence that the bubble plumes are directly related to breaking waves on the ocean surface.

Chapter 2

Summary of Principles of Acoustic Scattering from Bubbles

2.1 Sound Scatter from a Single Bubble

Consider an acoustic wave of frequency f_i impinging on a spherically-shaped bubble of radius a. If the resonant frequency f_r of the bubble is at or near the acoustic frequency then the sound energy will be very effectively scattered and absorbed by the bubble. These interactions are referred to as resonant scattering and resonant absorption (we shall ignore in the following the complicated effects of multiple scattering from bubbles which become important for very large concentrations of bubbles - see for example Ma et al [1983]).

Sound scattering from bubbles will also be observed if the bubble radius is much greater than the wavelength of sound, $a \gg \lambda$. This is called geometric scattering and occurs because of the pressure gradients across the bubble surface and the difference in the acoustic impedance of the water and that of the bubble gas ($\rho_w c_w$ and $\rho_g c_g$, respectively, where ρ_w and c_w are the density and speed of sound in water and ρ_g and c_g are the corresponding parameters for the

bubble gas). Significant geometric scattering does not occur for bubbles whose radii are much smaller than the acoustic wavelength, $a \ll \lambda_1$, because the instantaneous pressure across these bubbles is nearly uniform (although the presence of the bubbles does result in frequency dispersion of the sound waves [Clay and Medwin 1977]).

The degree of interaction between the bubble and the acoustic wave is described in terms of the absorption cross-section $\sigma_a = I_a/I$, the scattering cross-section $\sigma_s = I_s/I$, and the extinction cross-section $\sigma_e = \sigma_a + \sigma_s$. Here, I is the incident sound intensity at the bubble and I_a and I_s denote the total acoustic power absorbed and scattered by the bubble.

For an ideal bubble, the radius and resonant frequency are related through (Medwin 1977b)

$$f_r = \frac{1}{2\pi a}\left(\frac{3\gamma b T P}{\rho_\omega}\right)^{1/2} \qquad (2.1)$$

where

$$T = 1 + \left(\frac{2\tau}{\rho_\omega a}\right)\left[1 - \frac{1}{3\gamma b}\right]$$

$$b = \frac{1}{1+D^2}\left[\frac{1}{1 + \frac{3Y(\gamma-1)}{XZ}}\right]$$

$$X = a(2 f_r \rho_g C_p / K)^{1/2}$$

$$Y = \sinh X - \sin X$$

$$Y' = \sinh X + \sin X$$

$$Z = \cosh X - \cos X$$

$$D = 3(\gamma-1)\left[\frac{XY'-2Z}{X^2Z+3(\gamma-1)XY}\right].$$

Thus, a and f_r depend upon the ambient water density ρ_w, the surface tension at the air-sea interface τ, the ambient pressure P, the density of gases in the bubble ρ_g, their thermal conductivity K, their specific heat at constant pressure C_p and their ratio of specific heats γ.

The scattering cross-section for an ideal bubble is given by (U.S. Department of the Navy, 1969)

$$\sigma_s = \frac{4\pi a^2}{[(f_r/f_i)^2-1]^2+\delta^2} \qquad (2.2)$$

where $k_i=2\pi/\lambda_i$ is the acoustic wavenumber and δ is the total damping coefficient of the bubble. Devin (1959) determined the functional form of δ for bubbles at resonance. Eller (1970) obtained the more general relation

$$\delta = k_i a + D\left(\frac{f_i}{f_r}\right)^2 + \frac{4\mu}{\rho_w f_i a^2} \qquad (2.3)$$

(where μ is the shear viscosity of water) which is valid for bubbles which are not resonant at the acoustic frequency. The total extinction cross-section is further related to σ_s by (Eller 1970)

$$\sigma_e = \sigma_s\left(\frac{\delta}{k_i a}\right). \qquad (2.4)$$

Contaminants on the surface of the bubble can affect its acoustic properties. Theoretical studies indicate that the presence of such contaminants will increase the resonant frequency of a bubble

(Glazman 1983). In addition, the damping constant is increased at frequencies well below the resonant frequency, while at higher frequencies the damping constant is decreased (Glazman 1984). However, studies have not yet reached a state where we can estimate the extent of these effects in the ocean. We shall assume the bubbles are 'clean'.

2.2 Sound Scatter from Many Bubbles

Since a distribution of bubbles of different radii will exist at sea, one must take into account the scattering and absorption over the entire range of bubble sizes. We now consider a monochromatic acoustic wave impinging on a volume of bubbles. The net backscattered cross-section per unit volume (or scattering cross-section per unit volume per unit solid angle) is defined as

$$S_s = \frac{1}{V}\int_0^\infty \sigma_{bs}(a)\, n_v(a)\, da = \frac{1}{4\pi}\int_0^\infty \sigma_s(a)\, n(a)\, da \quad (2.5)$$

where V is the volume containing the bubbles, $\sigma_{bs}=\sigma_s/4\pi$ is the backscattered cross-section per unit volume for a single bubble, $n_v(a)$ is the number of bubbles within the entire volume with radii between a and a+da, and n(a) is the number of bubbles per unit volume with radii between a and a+da. Similarly, the net backscattered

extinction cross-section per unit volume is defined as

$$S_e = \frac{1}{4\pi} \int_0^\infty \sigma_e(a)\, n(a)\, da \,. \qquad (2.6)$$

If the acoustic wave takes the form of a pulse whose volume is less than that containing the bubbles, then the scattering volume is determined by the pulse volume. We consider an acoustic point source with a finite beam angle Ω (in steradians). The source is assumed to be directed towards a large volume of bubbles and to transmit a pulse of duration T at frequency f_i. The length of the pulse in the water is $L=c_w T$. For backscatter, however, the effective length is L/2.

At a particular range r from the source, determined by the instantaneous position of the center of the acoustic pulse at a time t/2 (where t is the two-way travel time), the volume of bubbles that contributes to scattering and absorption is defined by r, and L. For backscatter, the scattering volume is

$$V = \frac{\Omega}{3}\left[\left(r+\frac{L}{4}\right)^3 - \left(r-\frac{L}{4}\right)^3\right]. \qquad (2.7)$$

2.3 The Sonar Equation

The sonar equation relates transmitted and received sound levels to properties of acoustic targets and of the medium of sound propagation. Historically, the parameters in this equation have been specified in logarithmic form on a dB scale. We shall define some of these parameters before presenting the sonar equation.

The source level SL of an acoustic system is a measure of the sound intensity at a reference distance from a transmitter. The standard unit for sound pressure is the micro-Pascal, μPa, and the source level is measured in dB (re 1μPa^2) at a distance of 1m from the transducer (although many in the acoustics community are slow to adopt these standards even today). For a calibrated transmitter, the source level is given by

$$SL = 10 \log_{10}(\overline{V_x^2}) + TVR \qquad (2.8)$$

where $\overline{V_x^2}$ is the mean squared voltage applied across the transducer electrodes. TVR refers to the transmit voltage response (in dB re 1μPa^{2}V^{-2}), which is a measure of the efficiency of the transducer in converting electrical energy to acoustic energy.

The receive level RL of an acoustic system is a measure of the

acoustic power observed at a receiver (given in dB re $1\mu Pa^2$) and is defined by

$$RL = 10 \log_{10} \left(\overline{V_R^2} - \overline{V_N^2} \right) - OCV \qquad (2.9)$$

where $\overline{V_R^2}$ is the mean squared voltage signal observed across the terminals of the transducer, $\overline{V_N^2}$ is the mean squared voltage associated with system noise, and the OCV (open circuit voltage, given in $V^2 \mu Pa^{-2}$) is a calibration parameter indicating the efficiency of the transducer in converting acoustical to electrical power.

As sound propagates away from a point source, the intensity decreases due to geometric spreading and absorption of energy by the water. The latter effect occurs through the dissociation of salt ions in the water and through viscous effects. The associated two-way transmission loss TL for backscatter (in dB re $1m^2$)is given by

$$TL = 2 \left[20 \log_{10} r + \alpha (r-1) \right] \qquad (2.10)$$

where α is the acoustic absorption coefficient for sea water. At 119kHz, it is approximately 4.6×10^{-2} dBm^{-1} (from Clay and Medwin,1977).

Transmission through bubbles also leads to sound attenuation. The (two-way) transmission loss due to the presence of bubbles, TL_b

(in dB) is given by (Medwin 1977a) as

$$TL_b = 2\int_0^r \alpha_b \, dr \qquad (2.11)$$

where

$$\alpha_b = 4.34\, S_e \quad (dB\,m^{-1}) \qquad (2.12)$$

is the coefficient of sound attenuation due to scattering and absorption by the bubbles.

The effective target strength TS (in dB re $1m^2$) of a volume of scatterers is a measure of how efficiently those targets scatter sound. It is related to the scattering cross-section per unit volume through the relation

$$TS = 10 \log_{10}(S_s V) \, . \qquad (2.13)$$

It is also related to the previously defined paraemters through the sonar equation, which for a monostatic configuration (i.e. the transmitter and receiver are one and the same) is given as

$$TS = RL + TL + TL_b - SL \, . \qquad (2.14)$$

Thus, the observed target strength is related to the difference in the transmitted and received signal strengths, with the attenuation of sound due to geometric spreading, absorption in the water and the presence of bubbles taken into account.

Chapter 3

The Acoustic System

Sound scattering from bubbles was but one of a number of acoustic experiments carried out on the submarine. Consequently, the acoustic instrumentation was designed to be flexible. A block diagram of the system is provided in figure 1, indicating the inter-relationships among the principal components. The system parameters are summarized in table 1.

The acoustic transducers used in these experiments were commercially-available units (model ITC-3003), built and calibrated by International Transducer Corporation. A typical beam pattern for these devices is shown in figure 2. The transducers each contain a single disc-shaped piezo-electric element. Each unit has an optimum operating frequency of 119kHz and a (3-dB-down) mainlobe beamwidth of about 10^{o}.

The transducers were mounted on the submarine as indicated in figure 3. One unit (referred to as unit H, or the horizontal transducer)was positioned 3.9m above the deck at the vertex of the tripod and aimed directly forward; another was set on the deck 3.5m in front of the first and pointed vertically (unit V, or the vertical transducer); a third (unit B, or the bow transducer) was mounted on

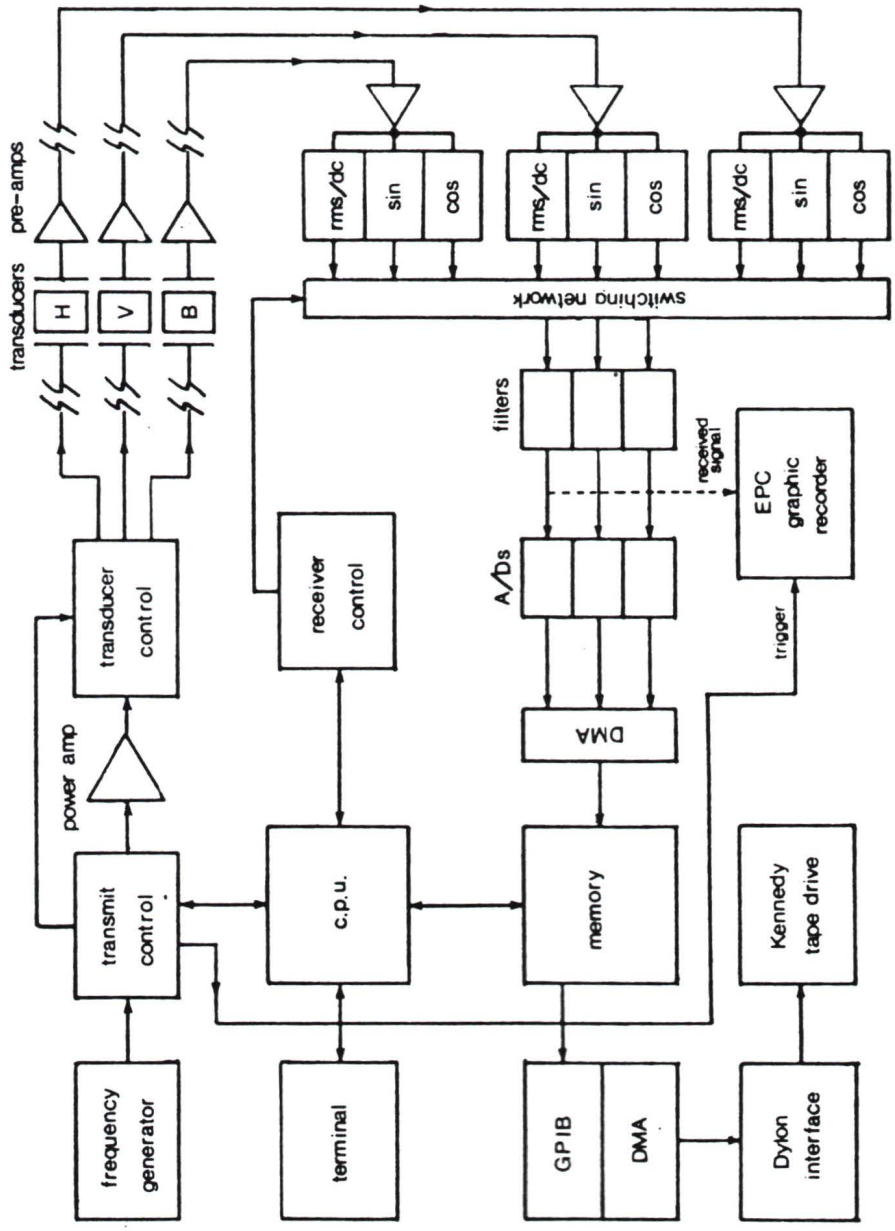

Figure 1 - Schematic diagram of the acoustic system used during the October 1984 DOLPHIN cruise.

Table 1 - Summary of Acoustic System Parameters

Operating frequency	119kHz
Beam width	10^{o}
Minimum pulse length	10^{-4}s
Number of data channels recorded	3
Maximum digitizing frequency (per channel)	25kHz
Maximum pulse repetition frequency	10Hz
Maximum output power	575W

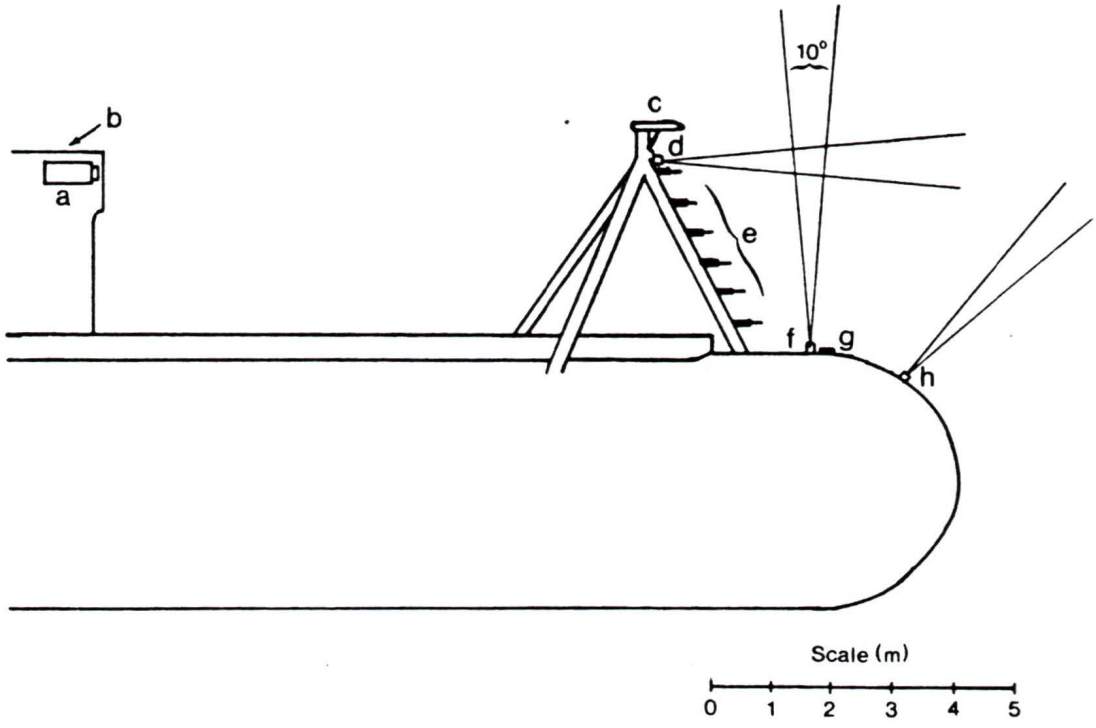

Figure 3 - Instrument deployment on the U.S.S. DOLPHIN during the October cruise: (a) 'bug-catcher'; (b) camera system (port side); (c) turbulence and microstructure probe package; (d) horizontal [H] transducer; (e) thermistor chain; (f) vertical [V] transducer; (g) acoustic doppler profiler; (h) bow [B] transducer.

the bow of the submarine and aimed forward at an angle of 45^{o} above the horizontal.

The transmission frequency was provided by a 119kHz frequency generator circuit. The output from this circuit was gated to form pulses, then passed through a power amplifier. Relays were used to direct the output from the power amplifier to the appropriate transducer. In order to minimize system noise, the relays would connect the appropriate transmit line to the power amplifier output for the duration of the transmit pulse only. Otherwise, all three transmit lines were disconnected from the system.

The signals received by the transducers were initially pre-amplified. The pre-amplifiers were placed in IOS-built aluminum pressure cases, which were attached to the transducers. Pre-amp power could be supplied from within the submarine or from battery sources also housed in the pressure cases. Inside the submarine, the received signals were further amplified and then de-modulated to provide amplitude and phase information. An amplitude signal was obtained by passing a received signal through an rms-to-dc converter; in-phase and quadrature phase signals were obtained by mixing a received signal with the 119kHz reference signal and with the reference signal phase-shifted by 90^{o}, respectively.

Although nine different signals (giving the amplitude, in-phase

and quadrature components for each of the three transducers) were produced, only three channels were recorded at a time. A switching network connected the desired channels to variable, low-pass analog filters. The outputs from the three filters were connected to sample-and-hold circuits, which in turn were used as inputs to high-speed 16-bit analog-to-digital (A/D) converters. The A/D outputs were transferred to computer memory. Because of high data sampling rates (up to 25kHz per channel), this transfer was performed using direct memory access (DMA).

The primary data recording system consisted of a Dylon magnetic tape controller and a 1600-b.p.i. Kennedy tape drive. Data were transferred from computer memory to the tape controller using DMA. The tape controller buffered the data and passed them to the tape drive. Data records were then written on 9-track computer tapes.

Data were also recorded in real-time on an EPC graphic recorder, which displays a four-bit digitized representation of the amplitude of a received signal as a function of time and of time delay (referenced with respect to the start of a pulse transmission). On the assumption that the sound speed is uniform (reasonable in most cases) and that the recorder inputs are selected for backscatter, this is equivalent to displaying the received signal as a function of range to the scatterers and time. The result is therefore an image of the scatterers in space and time.

Operation of the acoustic system was controlled using a Compupro micro-computer with a Z80 microprocessor. Due to the nature of these experiments, it was often necessary to adjust system parameters in order to meet changing environmental and observational requirements. To facilitate this, a menu-driven computer program was written to manage the acoustic system. The user was able to select the transmitting unit, whether it be a single transducer or a cyclic combination of two or of all three transducers. Two different modes were available for the recording of received signals, referred to as the intensity and complex modes. In the intensity mode, the amplitude signals from all three transducers were digitized. In the complex mode, the amplitude, in-phase and quadrature channels for the transmitting transducer were digitized (i.e. 180^{o} backscatter data only). Other software-controlled parameters included: pulse width, or duration of a pulse; transmission power; repetition rate of the pulses; sampling (digitizing) frequency; delay time and sample time, which define the 'window' over which data sampling takes place (referenced with respect to the start time of the transmission of the pulse).

Chapter 4

Observations and Analysis

Experiments were conducted on board the submarine USS DOLPHIN. Operations were carried out in the vicinity of 36^{o} 45'N, 122^{o}05'W, about 10km offshore from Monterey, California (see figure 4). Initial testing of the acoustic system took place during a preliminary cruise in April 1984. Following this, the system was modified to the form described in the previous section. The acoustic data described in this thesis were collected during thirteen dives occurring between October 3 and October 19, 1984.

During these dives, simultaneous measurements of turbulence and temperature (Dr. T. Osborn, Naval Postgraduate School) and of vertical current structure and ship speed (Dr. T. Stanton, Naval Postgraduate School) were obtained. In addition, during the final few dives, a 'bug-catcher' (Dr. L. Haury, SCRIPPS) and a camera system (Dr. D. Colton, Naval Postgraduate School) were in operation (see figure 3). A number of other parameters, including ship direction and sound speed, were monitored and recorded by instrument packages provided by the submarine. Meteorological data were obtained from the coast guard station at Point Pinos. We note that all times in this report refer to Pacific Daylight Time (PDT), which

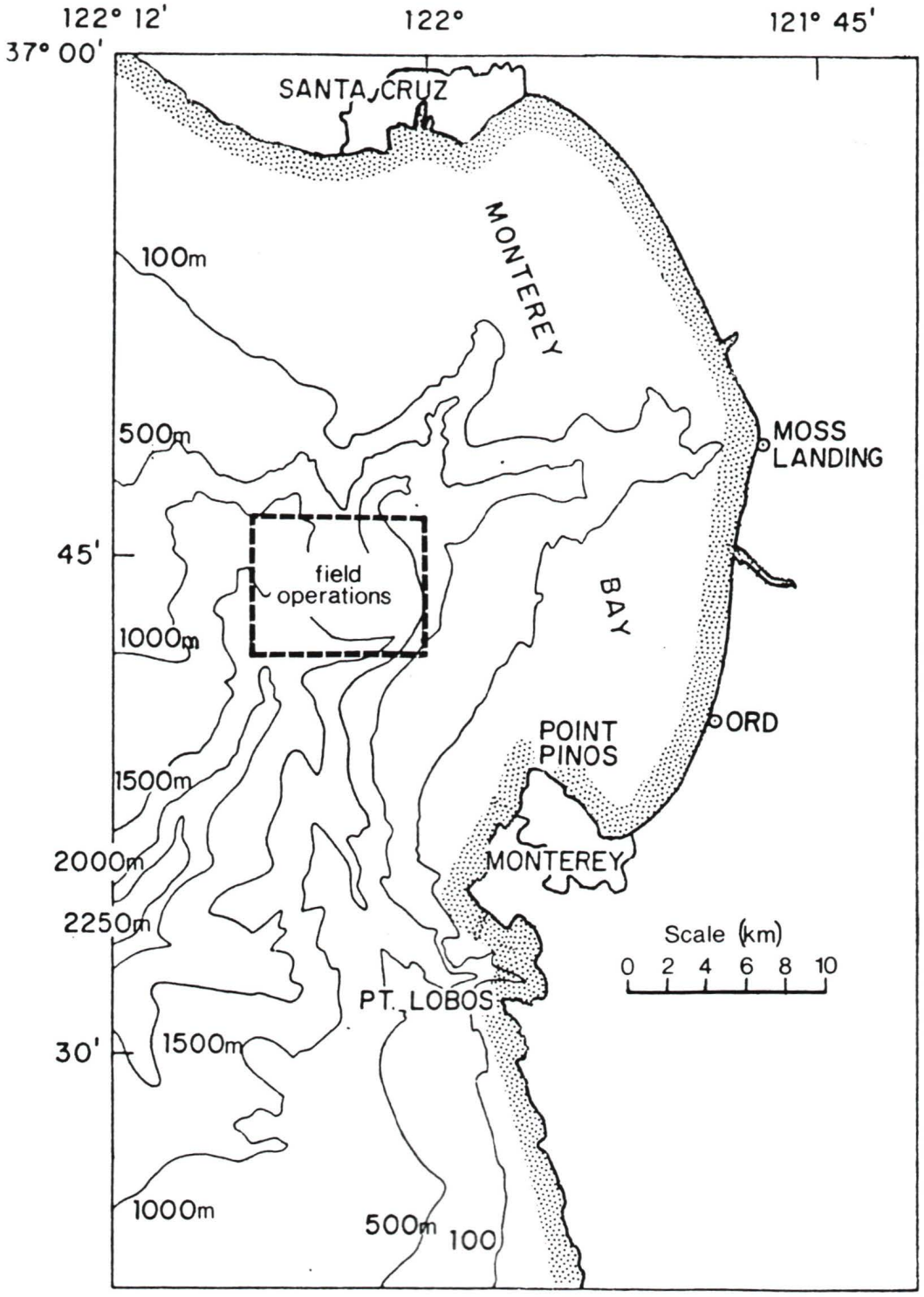

Figure 4 - Bathymetry along the coast of Monterey, California (after R. Loueck, personal communication). The location of field operations is indicated.

lags Universal Time by eight hours.

An acoustic image is provided in figure 5, corresponding to backscatter levels observed at the vertical transducer. This data set was collected on October 17 between 0159 and 0201. We identify here some of the principal acoustic targets in these observations. In this and in following acoustic images, the degree of shading is linearly proportional to the amplitude of the received signal, but the gains and offsets have been chosen to make the illustrations more comprehensible. The data has not been corrected for spherical spreading or absorption.

Coherent 'bands' of scatter can be seen relatively close to the submarine (out to a range of about 9m for the vertical transducer). These bands were due to sidelobe scattering from the submarine. This occurred because the submarine is a much stronger acoustic target than the majority of other scatterers close to it. Even though most of the acoustic energy was transmitted within the mainlobe of a transducer and did not strike the boat, the low-level sidelobe scatter from the boat was observed to dominate backscatter at ranges close to the transducers.

Beyond this region of sidelobe contamination, large numbers of weak, discrete targets and groups can be seen. These scatterers are for the most part biological in nature. In order to be 'seen' by our

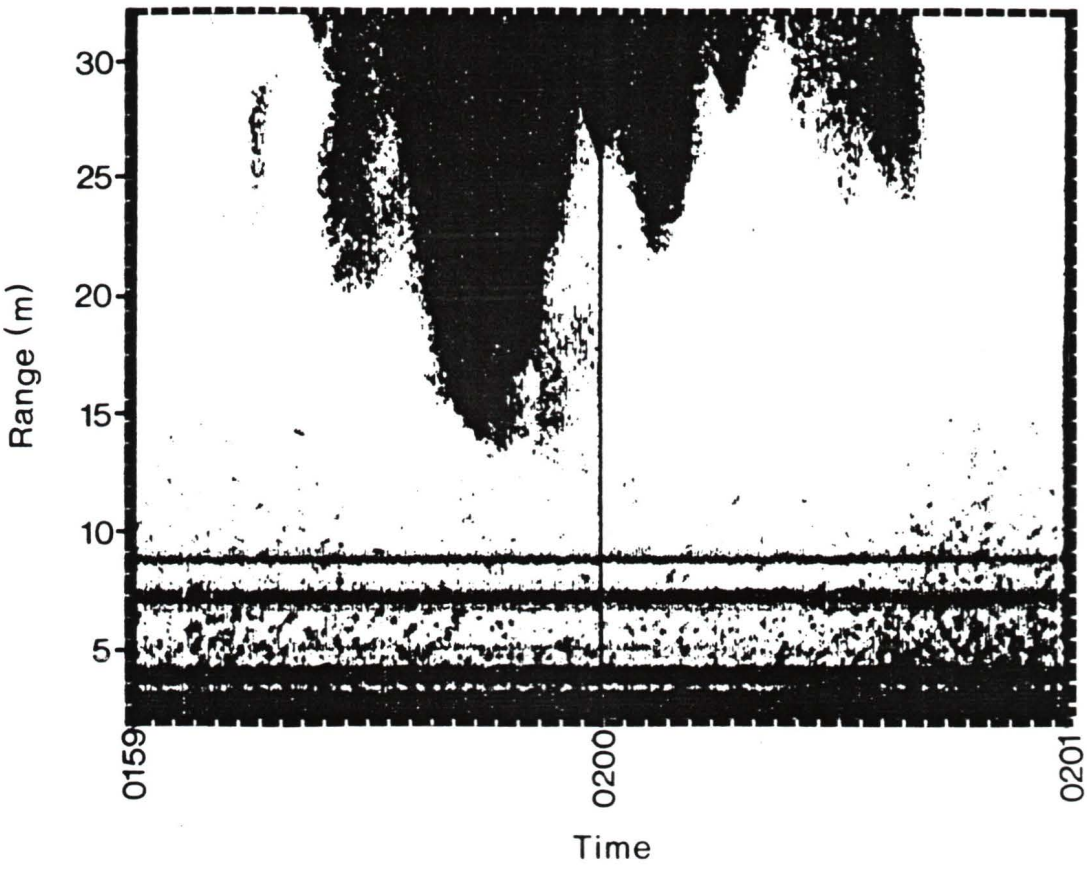

Figure 5 - An example of an acoustic image of backscatter observed at the vertical transducer. The broad lines are due to sidelobe scattering from the submarine. Discrete targets out to a range of about 12m are presumably plankton and other small scatterers. The 'plume-like' shapes at the top of the image are due to bubbles. The data were collected on October 17, 1984.

119kHz acoustic system, these targets must be of the order of our transmission wavelength (about 1.3cm) or larger. Previous acoustic studies in the ocean (e.g. Holliday and Pieper, 1980) have indicated these scatterers are primarily euphausiids and copepods. Biological samples taken during the October cruise confirmed that large numbers of copepods and euphausiids were often present, particularly at night (Dr. L. Haury, personal communication). During the day, the biota remain fairly deep, but at dusk they migrate towards the surface. Much stronger targets, appearing as either individuals or small discrete groups, were also occasionally observed in the water column. These were usually presumed to be small fish.

The biological targets in figure 5 appear to 'fade' with increasing distance from the transducer. This is primarily due to the geometric spreading loss in acoustic power. The power which reaches a target at a range r has decreased by a factor of r^{-2} compared with the power at a unit distance from the transducer. Similarly, the level of backscatter received from that target at the same transducer has also decreased by the same factor (assuming the targets scatter sound in an omnidirectional manner). There is thus an inherent range dependence of r^{-4} on backscattered power levels.

Large plume-shaped targets appear in figure 5. They are images of bubble clouds. The bubbles obviously represent a relatively strong acoustic target, in consideration of losses due to the

geometric spreading. In addition, few biological scatterers can discerned in the image at the associated range to the cloud. It is apparent they do not contribute significantly to the backscatter from the bubbles.

Another acoustic image of bubble clouds is provided in figure 6. Here the region of scatter from bubbles lies wholly within the data sampling window. The surface itself is a nearly perfect acoustic reflector, so sound that strikes the surface is reflected back down with little loss in power. However, the surface is not easily identified in figure 6 because of the presence of a 'mirror image' of the bubbles above the surface. This was observed to occur for strong transmission pulses. The acoustic path for the mirror image corresponds to sound which is reflected by the surface, impinges on the bubbles on the way down, scatters back to the surface and is reflected back down to the receiver. This concept is supported strongly in figure 6 by the presence of a large discrete target just below the surface (labelled A in the figure) and its twin (A') above the surface. The target was presumably a closely-packed school of fish. The undulations in the mirror image are due to the passage of waves on the surface.

Bubble observations made during the DOLPHIN cruise were referenced to the location of the vertical transducer. In order to reference the data to the surface, it was necessary to determine the

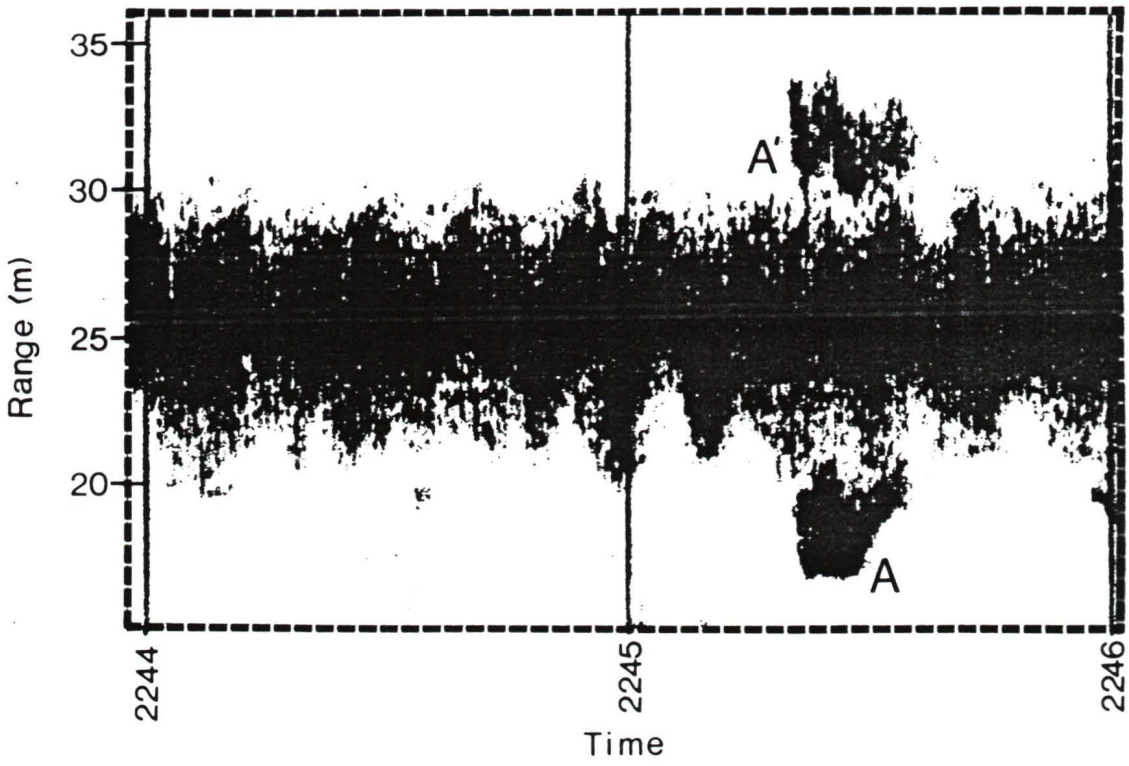

Figure 6 - An example of near-surface acoustic backscatter. The surface is not easily identified because of the presence of a mirror image of bubble clouds near the surface. A large target (perhaps a large fish or a closely-packed school of small fish) and its mirror image above the surface are labelled A and A', respectively. The data were collected on October 10, 1984.

range to the surface from the vertical transducer as a function of time. Surface reverberation was observed to saturate the digitally recorded signal for a few hundreds of microseconds during vertical transmission. An example of this is shown in figure 7. Acoustic scatter from bubbles near the surface is shown in figure 7a; in figure 7b, the same data set is plotted, but only saturated data points are shown. The relatively regular fluctuations in the surface reverberation layer are due to the passage of waves on the surface; very slow variations are attributed to the submarine diving or ascending. The wind speed for this data set was about $11 ms^{-1}$.

It was assumed that the range to the bottom of the surface reverberation layer corresponded to the instantaneous height of the surface directly above the vertical transducer. The range to the surface was then determined as a function of time for several sets of data. Using this time series, it was possible to re-plot acoustic images without the complication of mirror images lying above the surface. Such an image is plotted in figure 7c. Data 'beyond' the surface have been inhibited in this figure.

There is clearly a correlation in figure 7c between the variation of the surface level and that of the bottom of the bubble clouds. Thus, the surface waves can modulate the bubble distribution significantly, a result which is consistent with previous acoustic observations made by Aleksandrov and Vaindruk(1974). This does not

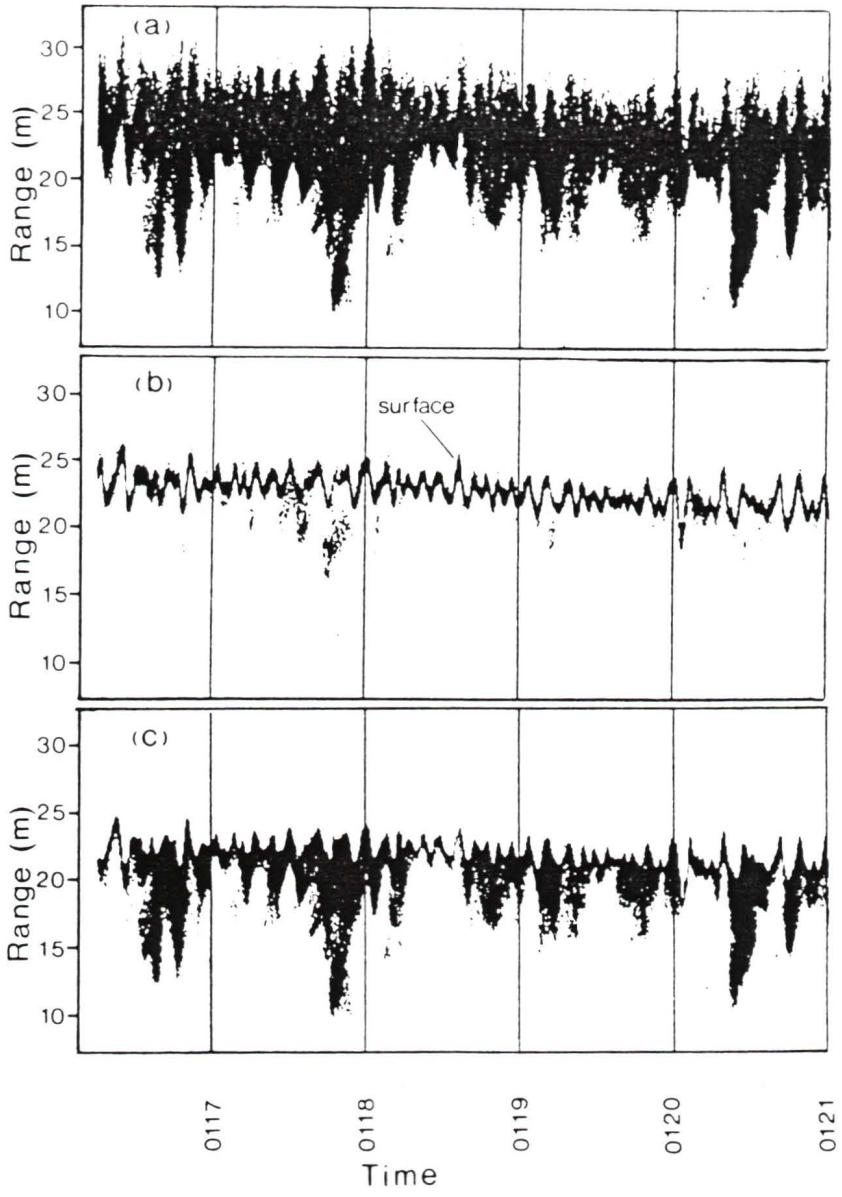

Figure 7 - Removing mirror images from the acoustic data: (a) the raw received data; (b) data which saturated the receiving electronics; (c) the raw data re-plotted, with suppression of data beyond the surface. The data were collected on October 17, 1984.

mean, however, that the waves and the bubble clouds have similar length scales. The bubble clouds are relatively fixed with respect to the ocean, while the waves are propagating along the surface. We must look more closely in order to determine the length scales of the surface waves.

Time series of wave height estimates were determined by high-pass filtering time series of the range to the surface, thereby removing the mean distance to the surface and the effects of vertical submarine motion; one-dimensional wave height spectra were obtained by Fourier-transforming time series of wave height. For data sets collected at relatively constant horizontal ship speed, the one-dimensional power spectra of wave height tended to show a dominant frequency band (for example, see figure 8), consistent with the relatively periodic surface undulations indicated in figure 7b.

It should be noted that wave height spectra evaluated with a finite beam transducer will not be accurate at high frequencies. The finite beam acts as a low-pass filter in measurements of the range to the surface. This process is indicated in figure 9a. We first consider a low-frequency wave whose wavelength λ is much greater than the length of the acoustic 'footprint' h (i.e. the diameter of the circular area at the surface encompassed by the beam). In this case, the shortest distance to the surface is along the vertical axis and a time series of range to the surface represents accurately the surface

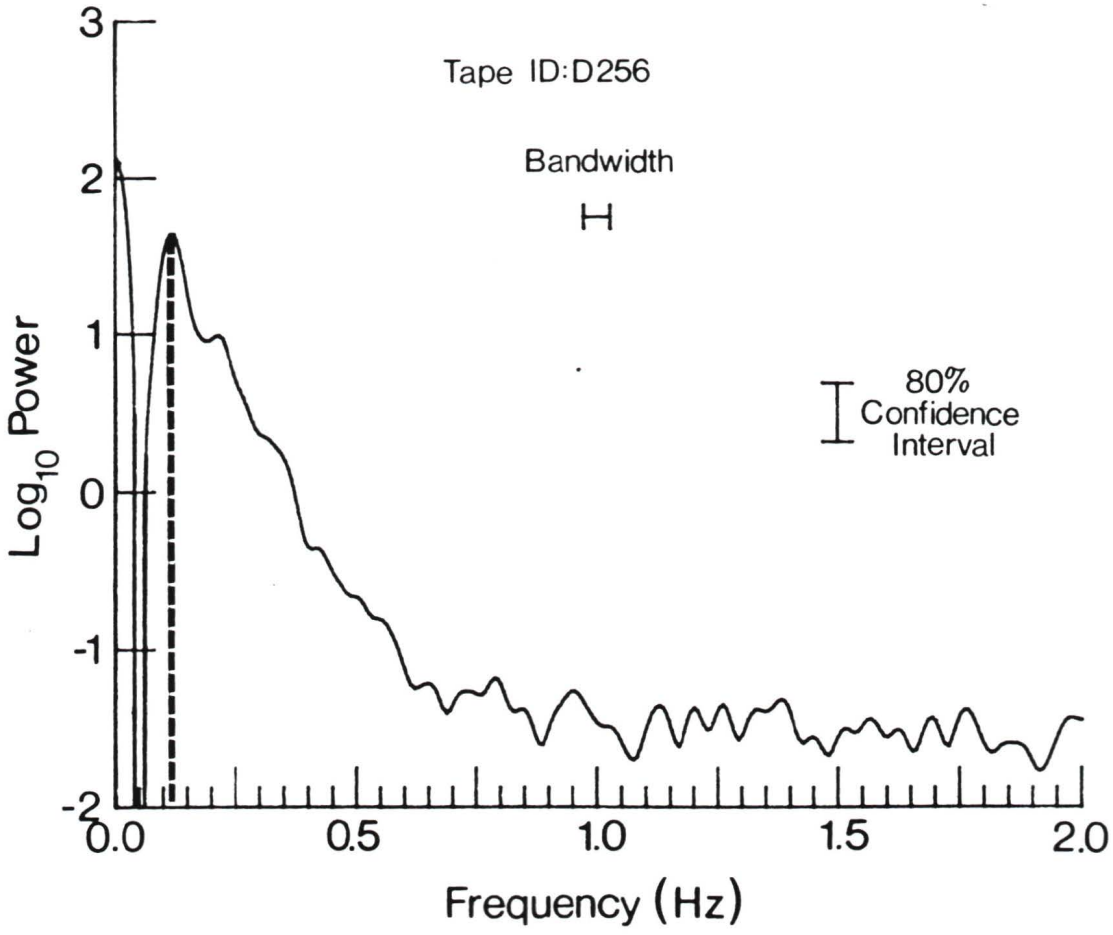

Figure 8 - A sample power spectrum of the surface, with the peak occurring at about 0.13Hz. Power is in arbitrary units. The submarine was travelling with the wind at about $1.4ms^{-1}$. The corresponding wavelength of swell, from equation (4.3), is about 120m.

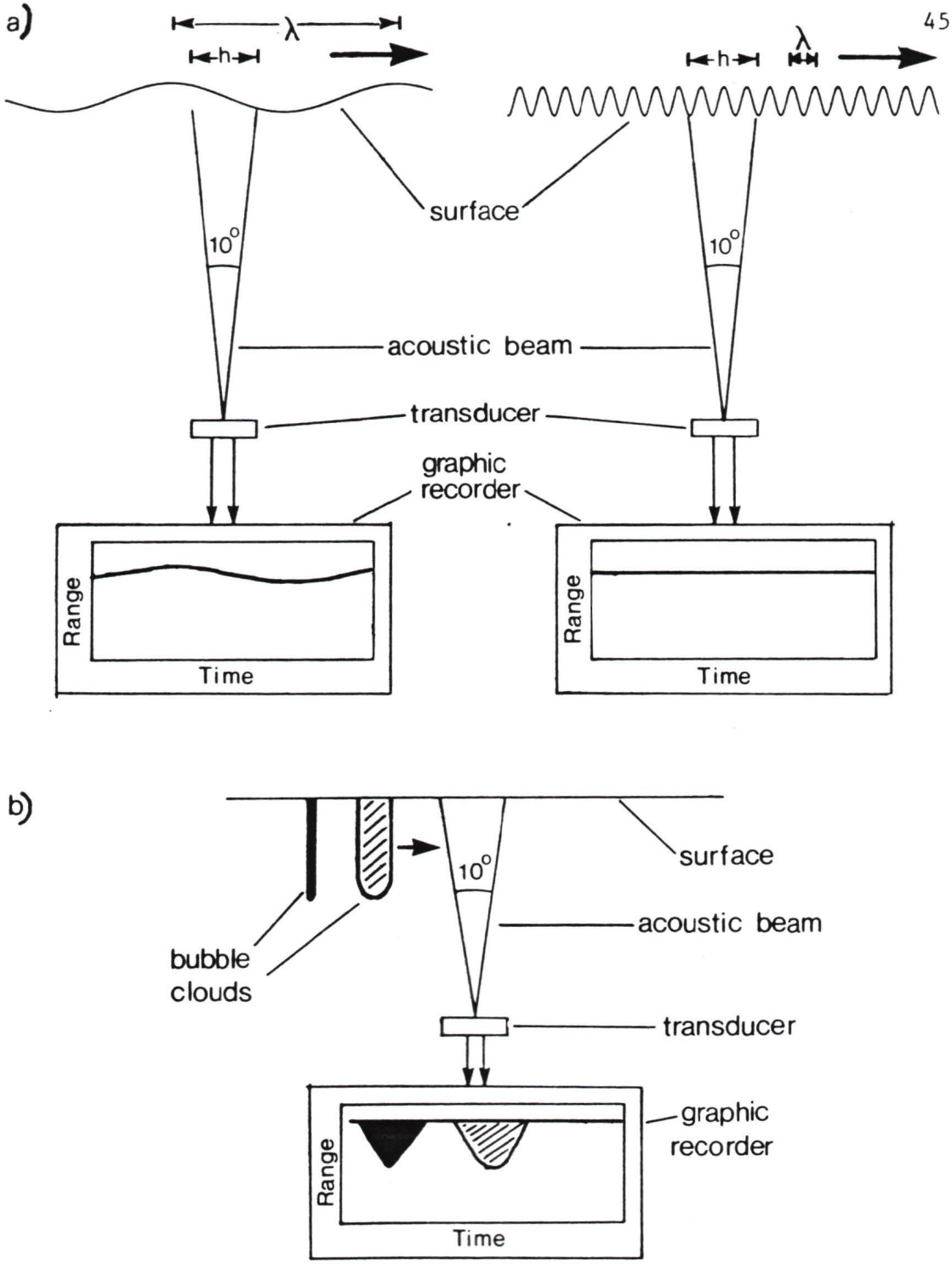

Figure 9 - Finite beam effects: (a) surface waves whose wavelength λ is much greater than the acoustic footprint h are resolved by the acoustic system, whereas waves which are much shorter than h are not; (b) bubble clouds passing through the acoustic beam appear more 'spread out' at a given range by an amount proportional to the diameter of the beam at that range.

waveform. In contrast, for a high-frequency wave whose wavelength is much smaller than the acoustic footprint, the shortest distance to the surface will be the length of a line from the transducer to the wave trough nearest the vertical axis. This distance will not change much during propagation of the surface wave and the time series of the range to the surface will be nearly constant. The finite beam width also tends to broaden the apparent width of bubble clouds by an amount equal to the width of the acoustic beam at the depth of interest, as depicted in figure 9b.

The footprint of the sonar was typically 5m wide. Thus, waves whose frequencies were much less than about 0.56Hz are accurately represented in the wave height spectra. Swell frequencies are typically 0.1Hz and less, so swell was easily resolved.

Recall from equation (1.2) the dispersion relation for deep-water waves is given by

$$c = f\lambda = \left(\frac{g\lambda}{2\pi}\right)^{1/2} \qquad (4.1)$$

where c is the phase speed of the wave, g is gravitational acceleration, λ is the wavelength and f is the frequency of oscillation. This is for a reference frame fixed with respect to the ocean. The submarine, however, represents a reference frame moving at a speed v with respect to the ocean at some angle θ relative to the direction of propagation of the waves. The frequency of

oscillation of the surface as observed in this latter frame of reference is

$$f' = f\left(1 - \frac{V}{C}\cos\theta\right). \qquad (4.2)$$

Eliminating c, we find the wavelength of surface waves is given by the quadratic relation

$$\lambda^2 + \lambda\left[\frac{2V\cos\theta}{f'} - \frac{g}{2\pi f'^2}\right] + \frac{V^2\cos^2\theta}{f'^2} = 0. \qquad (4.3)$$

Equation (4.3) was used to estimate the length scale of the surface waves. Wave height power spectra, evaluated in the reference frame of the submarine using time series of the range to the surface, provided a means for determining the dominant frequency of surface variations. The direction of wave propagation was presumed to be in the direction of the wind. Ship velocity was taken to be in the forward direction of the ship (cross-stream speeds were typically much less than 10% of forward speeds [T. Stanton, personal communication] and were hence assumed to be negligible). The resulting wavelengths were between 150m and 250m, and had corresponding phase speeds of 15-19ms^{-1}. Such waves are in the regime of ocean swell. The total water depth was typically much greater than 500m. The corresponding error in using the deep water relation (equation (4.1)) for evaluating the wavelength of such waves is therefore much less than 0.1%.

This result brings into question the initial assumption that the waves were moving in the direction of the wind, since swell consists of free travelling waves which are generated at some distance from local atmospheric conditions. However, a number of observations still support the hypothesis. The transition from sea to swell is not a discrete one (Kinsman 1965). The observed wavelengths of the surface waves are at the low end of length scales associated with swell and are thus comparable to the locally-generated wind waves. Thus the swell may not have been generated very far from the local environment. Secondly, during the cruise the winds were blowing predominantly out of the north-west across an essentially unlimited fetch. It would therefore not be unreasonable to suggest the atmospheric forcing which generated the swell was oriented in the same direction as the local forcing. Finally, during one particular dive we used the periscope to allow us to run with the waves. The ship direction was found to line up with the wind direction during this period. Therefore, the assumption of identical direction of propagation for the wind and the observed surface waves is deemed a reasonable one.

In light of these results, it was possible to estimate the effects of the surface wave motion on the bubbles as a function of depth. The total water depth was usually quite large (typically greater than 500m) relative to the wavelength of the dominant surface

waves, which allowed us to make use of the deep-water relation for particle motion due to a sinusoidal surface wave (Pond and Pickard 1983), namely

$$w = \omega A \cos(kx - \omega t) \exp(-kz) \qquad (4.4)$$

where w is the vertical velocity of a fluid particle, x is the direction of propagation of the wave, z is the depth below mean surface level, t is time, and A, ω and $k=2\pi/\lambda$ are the amplitude, angular frequency and wavenumber of the wave respectively. This predicts an exponential decrease in the vertical displacement of particles with depth for a single-frequency wave.

We may determine the correction due to the displacement of the free surface from equilibrium by swell. The instantaneous range from the submarine to a depth z below the free surface, taking this correction into account, is then given by

$$r_z(t) = r_s(t) - z + A \exp(-kz) \qquad (4.5)$$

where $r_s(t)$ is the instantaneous range from the ship to the mean surface level (i.e. the low-frequency signal in the surface time series). Using this relation, bubble population estimates were referenced to depths below the surface.

Recall from equation (2.5) the acoustic backscattering cross-section per unit volume due to insonification (i.e. irradiation

with sound) of bubbles at some fixed frequency f_i is given by

$$S_s = \frac{1}{4\pi} \int_0^\infty \sigma_s(a,z)\, n(a,z)\, dz \qquad (4.6)$$

where $_s$ is the scattering cross-section per unit volume for a bubble of radius a at a depth z and n(a) is the corresponding density of bubbles with radii between a and a+da. Following Wu's (1981) analysis of bubble spectra obtained by Johnson and Cooke(1979), it is assumed that an equilibrium distribution exists in which the relative number of bubbles of a particular size is constant. Under this assumption equation (4.6) can be written as

$$S_s = \frac{N(z)}{4\pi} \int_0^\infty \sigma_s(a,z)\, p(a)\, da \qquad (4.7)$$

where N is the net density of bubbles and p(a)da is the normalized equilibrium (i.e. probability) distribution in m^{-3}. Similarly, the extinction cross-section per unit volume can be written as

$$S_e = \frac{N(z)}{4\pi} \int_0^\infty \sigma_e(a,z)\, p(a)\, da \,. \qquad (4.8)$$

For a given depth, the integrals in equations (4.7) and (4.8) are constant.

The probability distribution was modelled by the function

$$p(a) = \begin{cases} 0 & a < 17\mu m \\ -4.1\times10^{-5}(a-42)^2 + 2.56\times10^{-2} & 17\mu m \leq a \leq 58\mu m \\ 9.9\times10^{6}\, a^{-5} & 58\mu m < a \end{cases} \qquad (4.9)$$

where a is in μm and p(a) is in m^{-3} per 1μm band. A plot of this function is shown in figure 10 and is compared with the (appropriately normalized) results obtained by Johnson and Cooke. The dependence of p(a) on bubble radius for relatively large bubbles is consistent with a model proposed by Kerman(1982).

Recall from equation (2.12) the (two-way) attenuation of sound due to the presence of bubbles is given by

$$\alpha_b = 4.34\, S_e \qquad (4.10)$$

where α_b is in dBm^{-1}. From equations (4.7), (4.8) and (4.10) one can evaluate the attenuation of sound at a given depth from S_s

$$\alpha_b = 4.34\, S_s \frac{\int_0^\infty \sigma_e\, p(a)\, da}{\int_0^\infty \sigma_s\, p(a)\, da} \,. \qquad (4.11)$$

The integrals in equation (4.11) were evaluated numerically at a variety of depths. The results are plotted in figure 11. Both are seen to increase with depth. On the other hand, the ratio of the two integrals is not quite so sensitive to the depth, particularly within the first few meters of the surface. At 25cm depth, the ratio is approximately 4.8; at 5m, the ratio is about 4.5. Since the vast majority of bubbles are known to lie close to the surface, it was

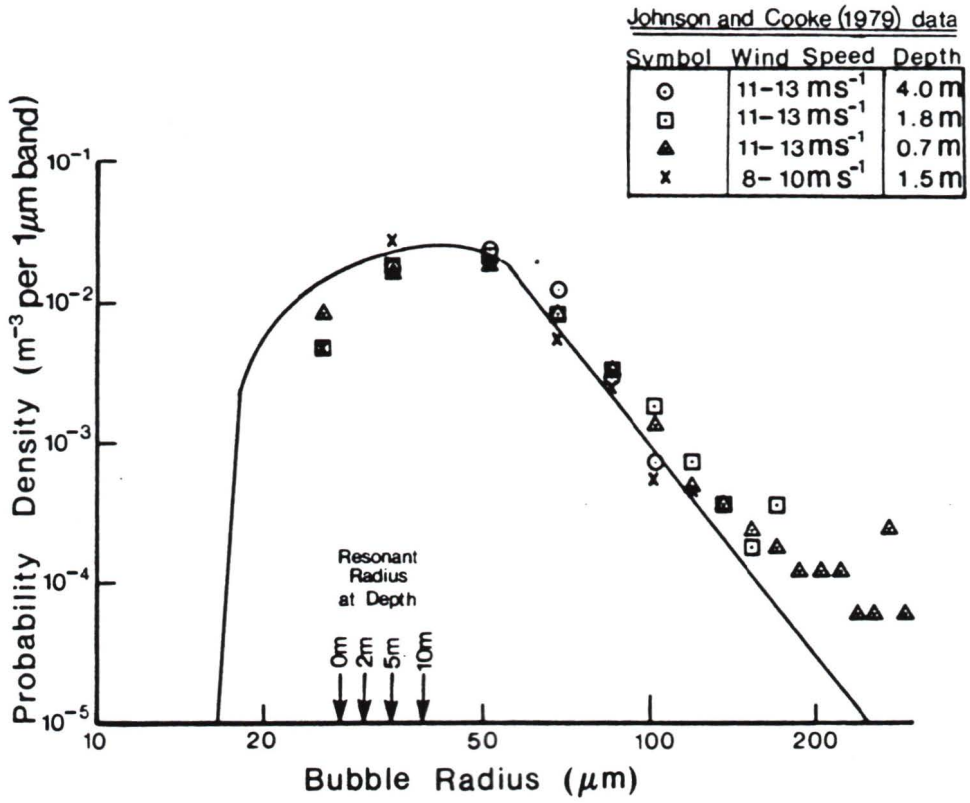

Figure 10 - A plot of the model used for the bubble size probability Observations by Johnson and Cooke (1979), appropriately normalized, are provided for comparison. The radius of bubbles which are resonant at 119kHz are indicated at 4 different depths.

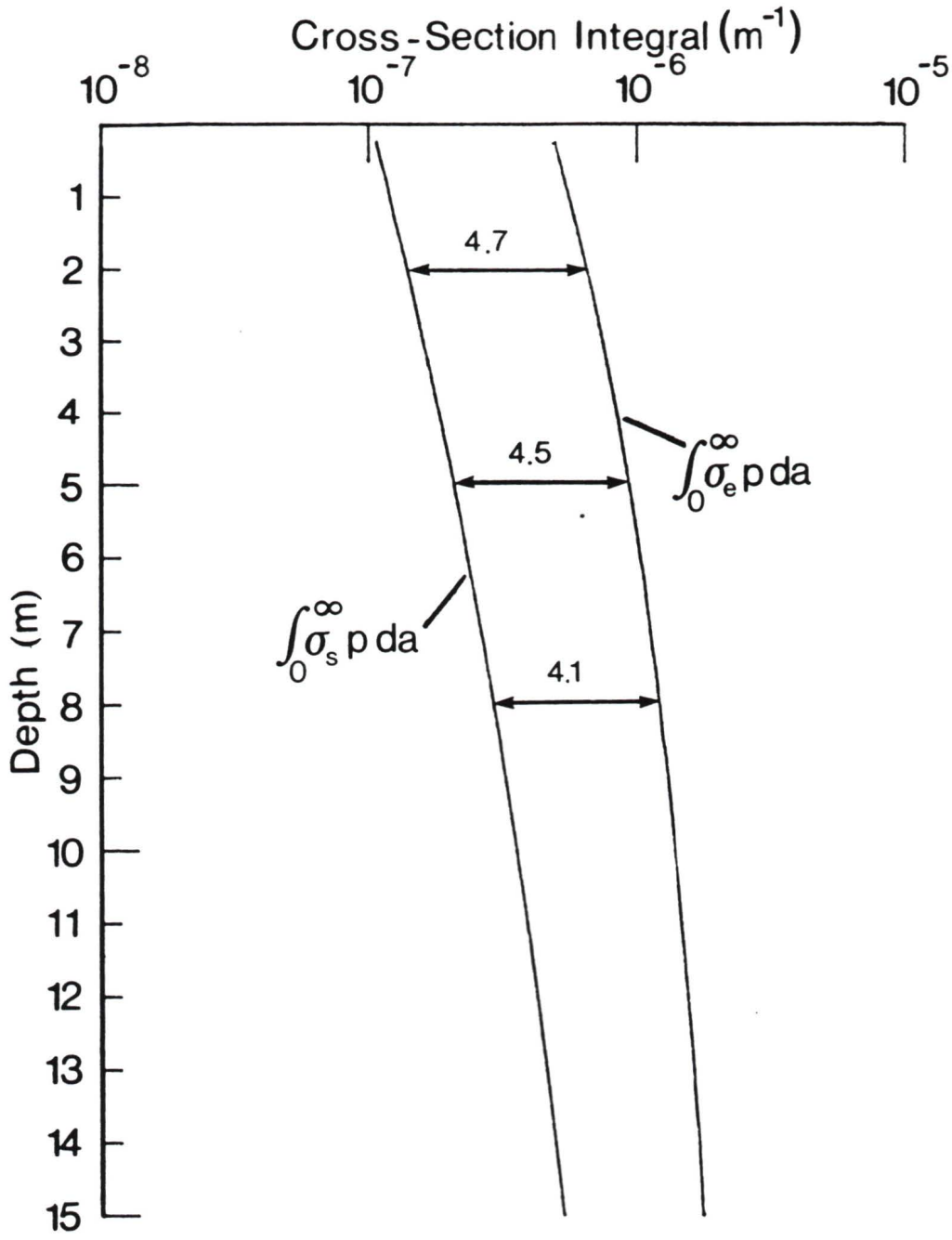

Figure 11 - Values of $\int_o^\infty \sigma_s p\ da$ and $\int_o^\infty \sigma_e p\ da$, evaluated numerically, are provided as a function of depth. The ratio of the two integrals is nearly constant within the first 5m below the surface.

assumed the ratio was constant. A representative value of 4.7 (corresponding to 2m depth) was used in calculations of α_b. Errors resulting from this assumption are limited to about 5% within the first 5m below the surface. The two-way transmission loss due to bubbles for acoustic propagation to a range r was calculated using the equation

$$TL_b = 4.7 \times 8.68 \int_0^r S_s(r)\, dr. \qquad (4.12)$$

Since S_s is also a function of TL_b (equations (2.13) and (2.14)), the net attenuation was path-integrated as a function of range for each transmission.

Values of S_s were determined using equations (2.13), (2.14) and (4.12) for each transmission. These values were averaged vertically over 25cm intervals (bins) to a depth of 15m below the surface and horizontally over 1-2m. Estimates of the bubble density for each depth bin were obtained using equation (4.7). Contours of the (common logarithm of the) bubble density were then plotted. In these contours, the effects of swell and of the vertical motion of the submarine have been removed.

Observations of the distribution of bubbles near the ocean surface under different conditions are provided in figures 12 through 19. Each figure contains graphic images of digitally-recorded acoustic returns and, where possible, contour plots of the associated

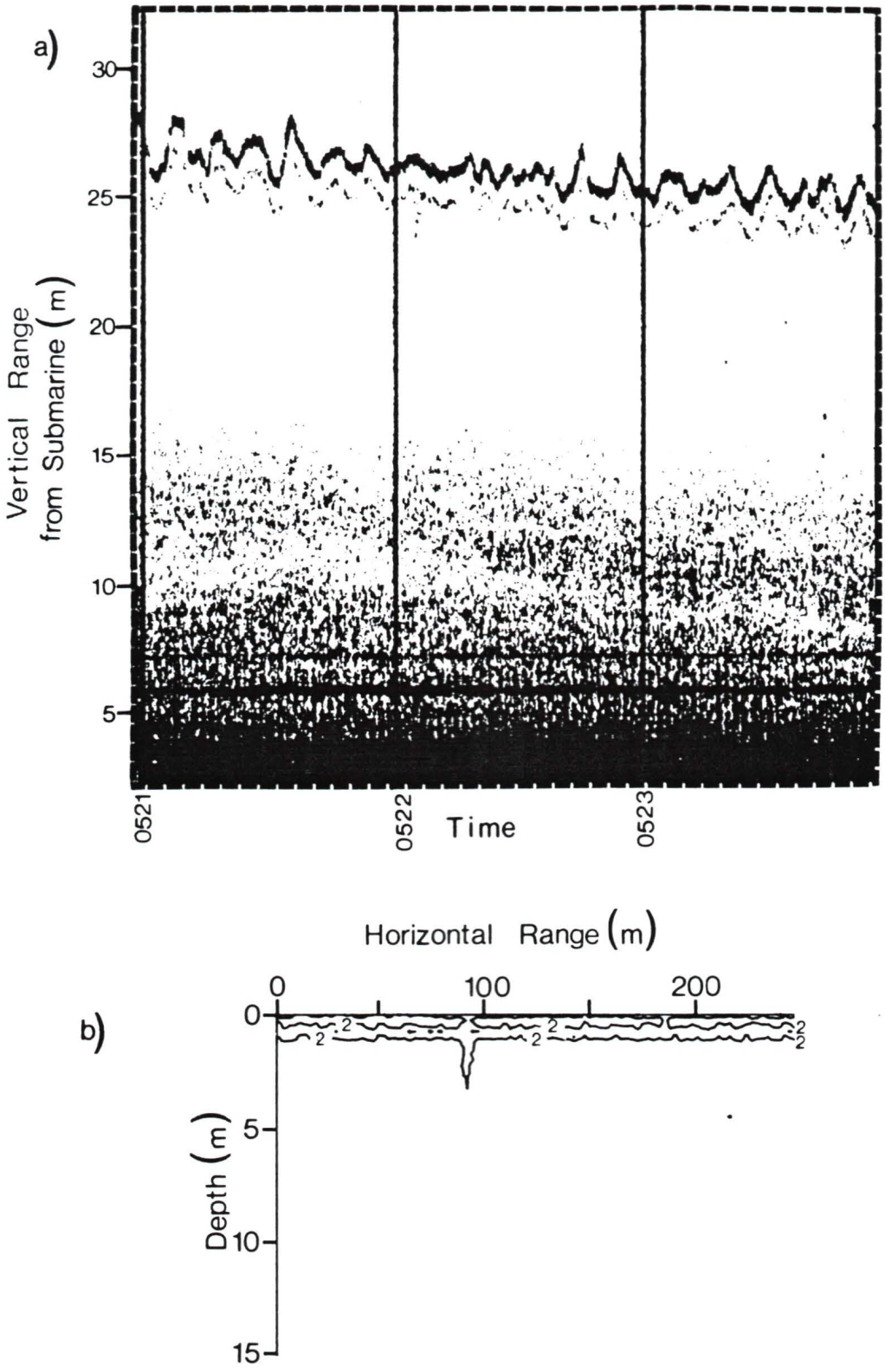

Figure 12 - Observations of the distribution of bubbles: (a) an acoustic backscatter image; (b) contour plot of the (logarithm of the) bubble concentration as a function of horizontal range and of depth (October 10; $U_{10}=3ms^{-1}$; $\theta=135^{o}$; ΔT=unknown).

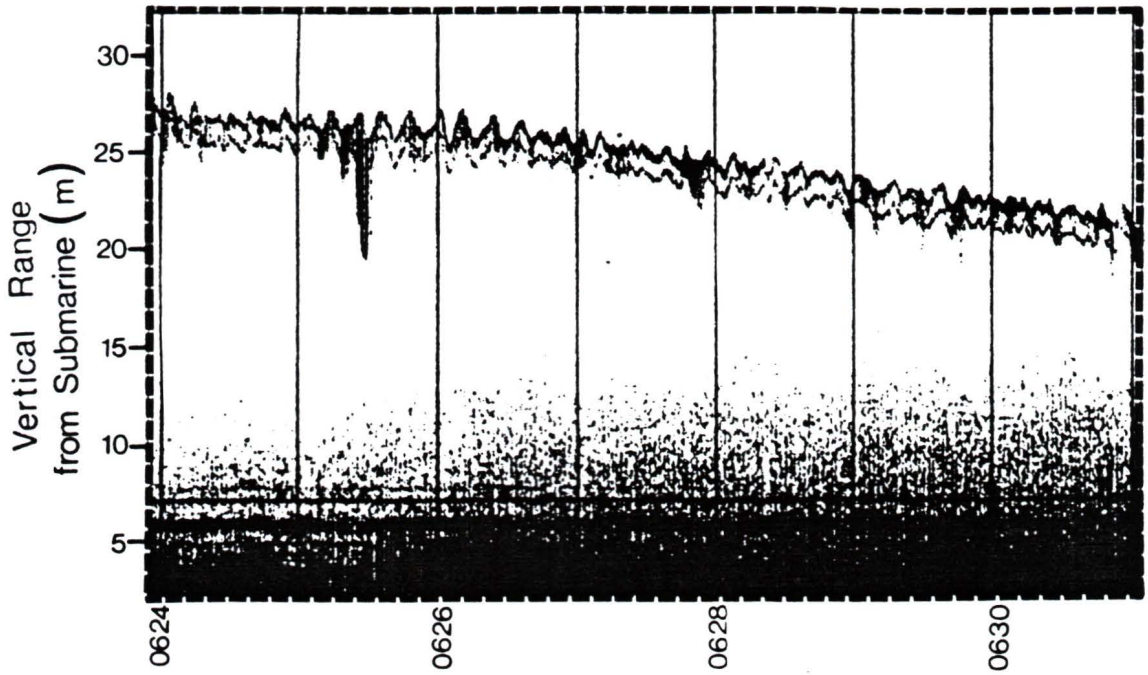

Figure 13 - Observations of the distribution of bubbles: an acoustic backscatter image (October 10; U_{10}=3ms $^{-1}$; θ=45^{o}; ΔT=unknown).

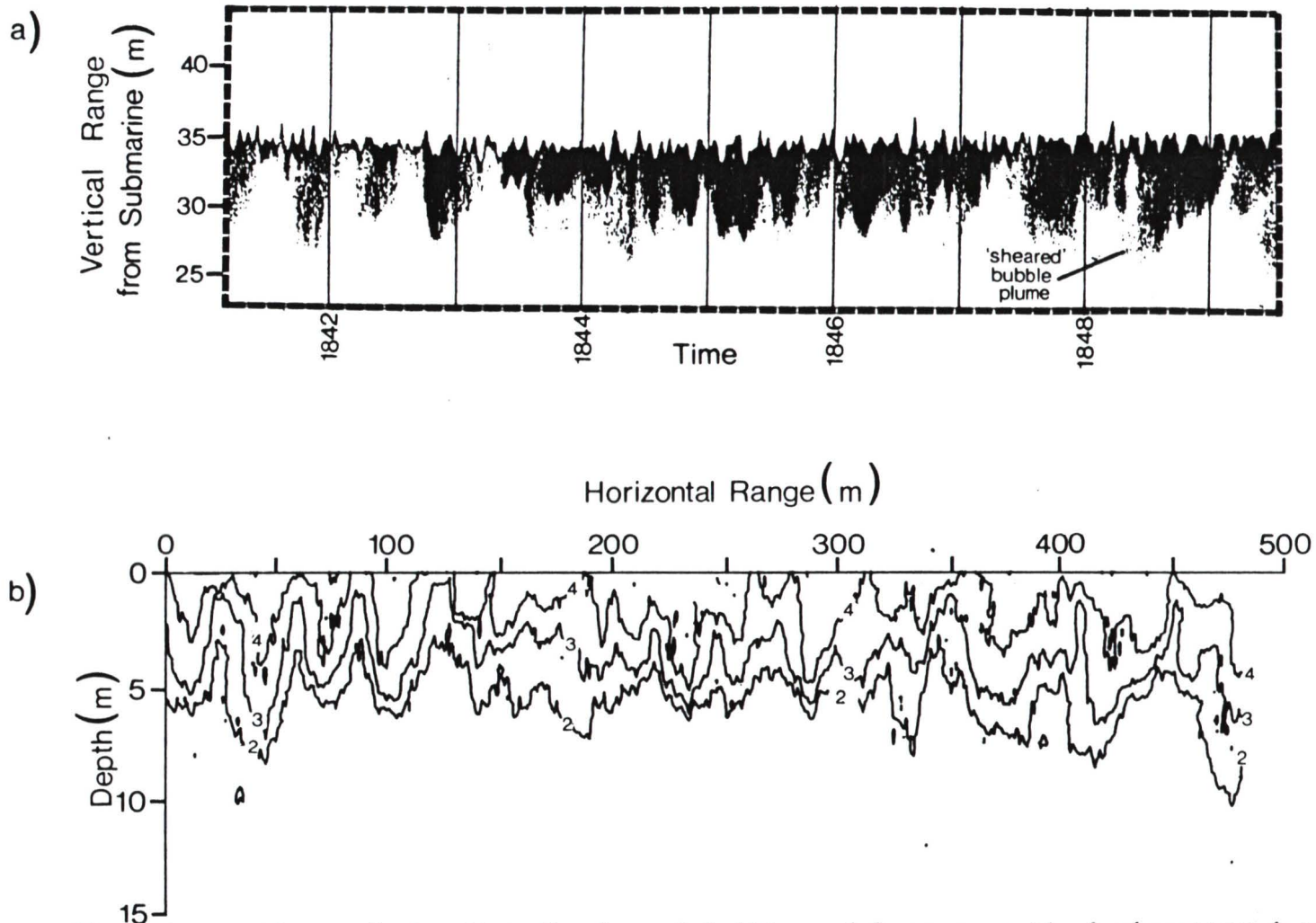

Figure 14 - Observations of the distribution of bubbles: (a) an acoustic backscatter image; (b) contour plot of the (logarithm of the) bubble concentration as a function of horizontal range and of depth (October 10; $U_{10}=8ms^{-1}$; $\theta=45^{o}$; $\Delta T=-1^{o}C$).

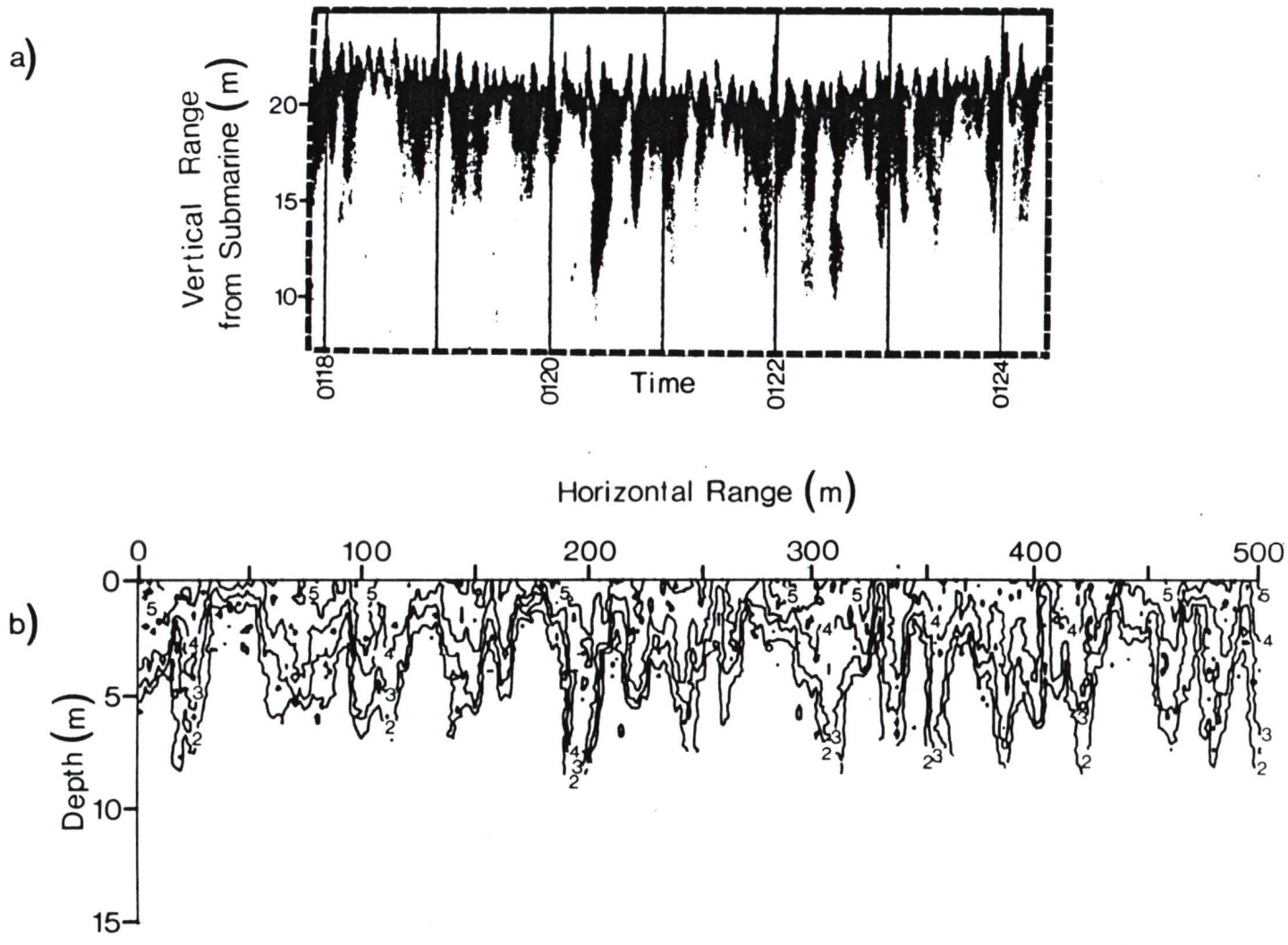

Figure 15 - Observations of the distribution of bubbles: (a) an acoustic backscatter image; (b) contour plot of the (logarithm of the) bubble concentration as a function of horizontal range and of depth (October 17; U_{10}=11ms $^{-1}$; θ=45^{o}; ΔT=-3.5^{o}C).

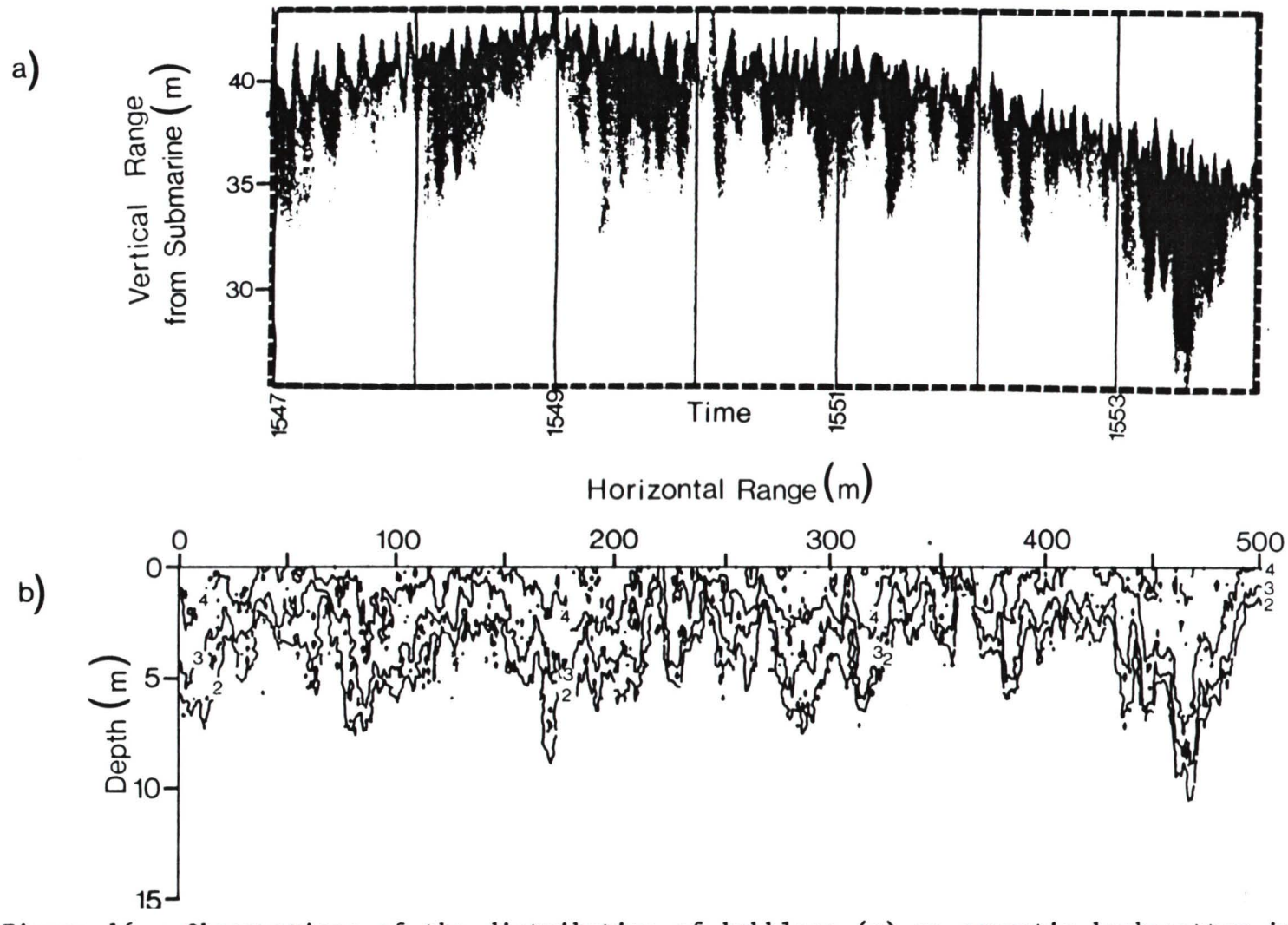

Figure 16 - Observations of the distribution of bubbles: (a) an acoustic backscatter image; (b) contour plot of the (logarithm of the) bubble concentration as a function of horizontal range and of depth (October 17; U_{10}=10ms $^{-1}$; θ=180^{o}; ΔT=-2.5^{o}C).

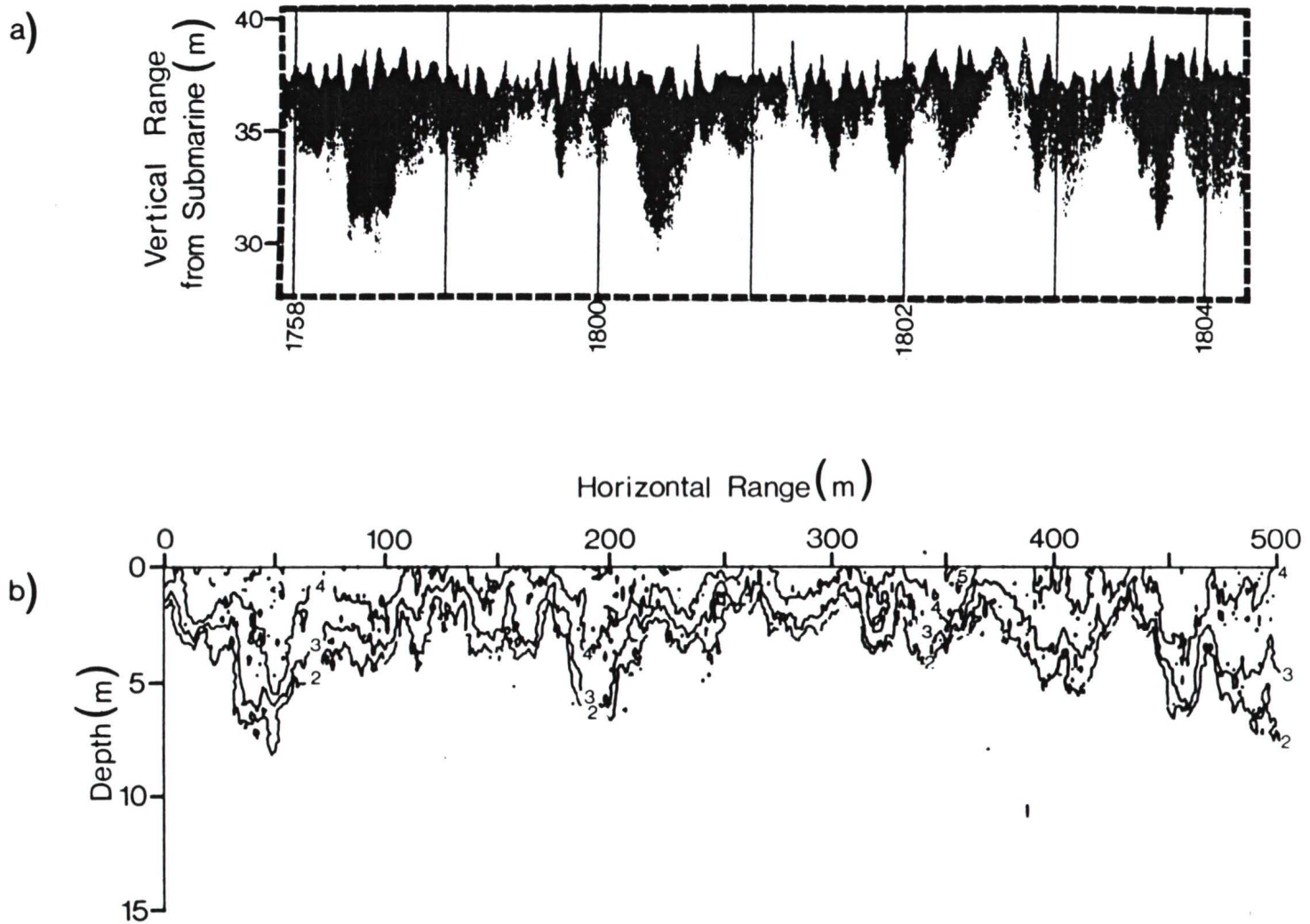

Figure 17 - Observations of the distribution of bubbles: (a) an acoustic backscatter image; (b) contour plot of the (logarithm of the) bubble concentration as a function of horizontal range and of depth (October 17; U_{10}=10ms^{-1}; θ=0^{o}; ΔT=-2.5^{o}C).

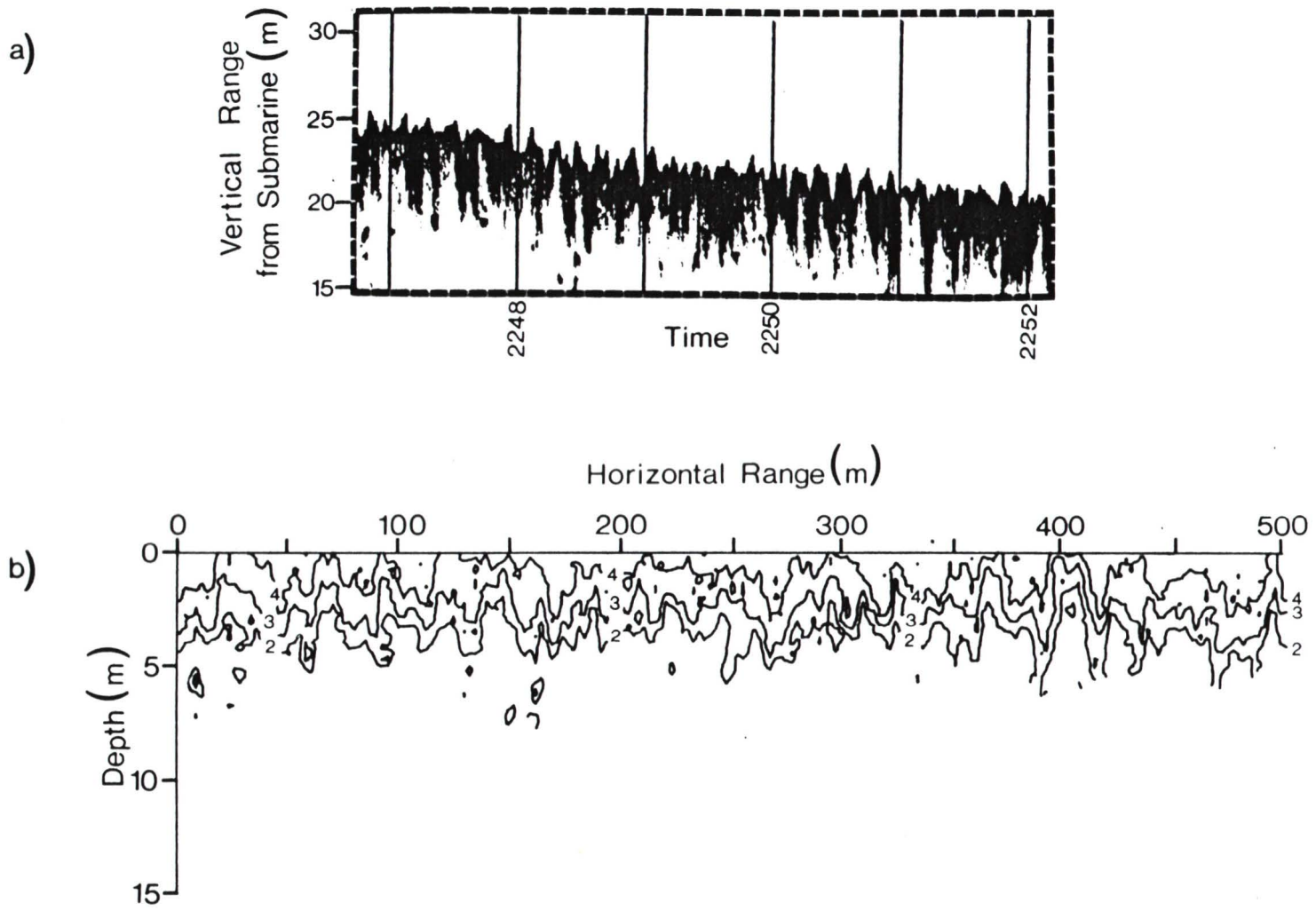

Figure 18 - Observations of the distribution of bubbles: (a) an acoustic backscatter image; (b) contour plot of the (logarithm of the) bubble concentration as a function of horizontal range and of depth (October 10; U_{10}=7ms $^{-1}$ (uncertain); θ=135^{o}; ΔT=-1^{o}C).

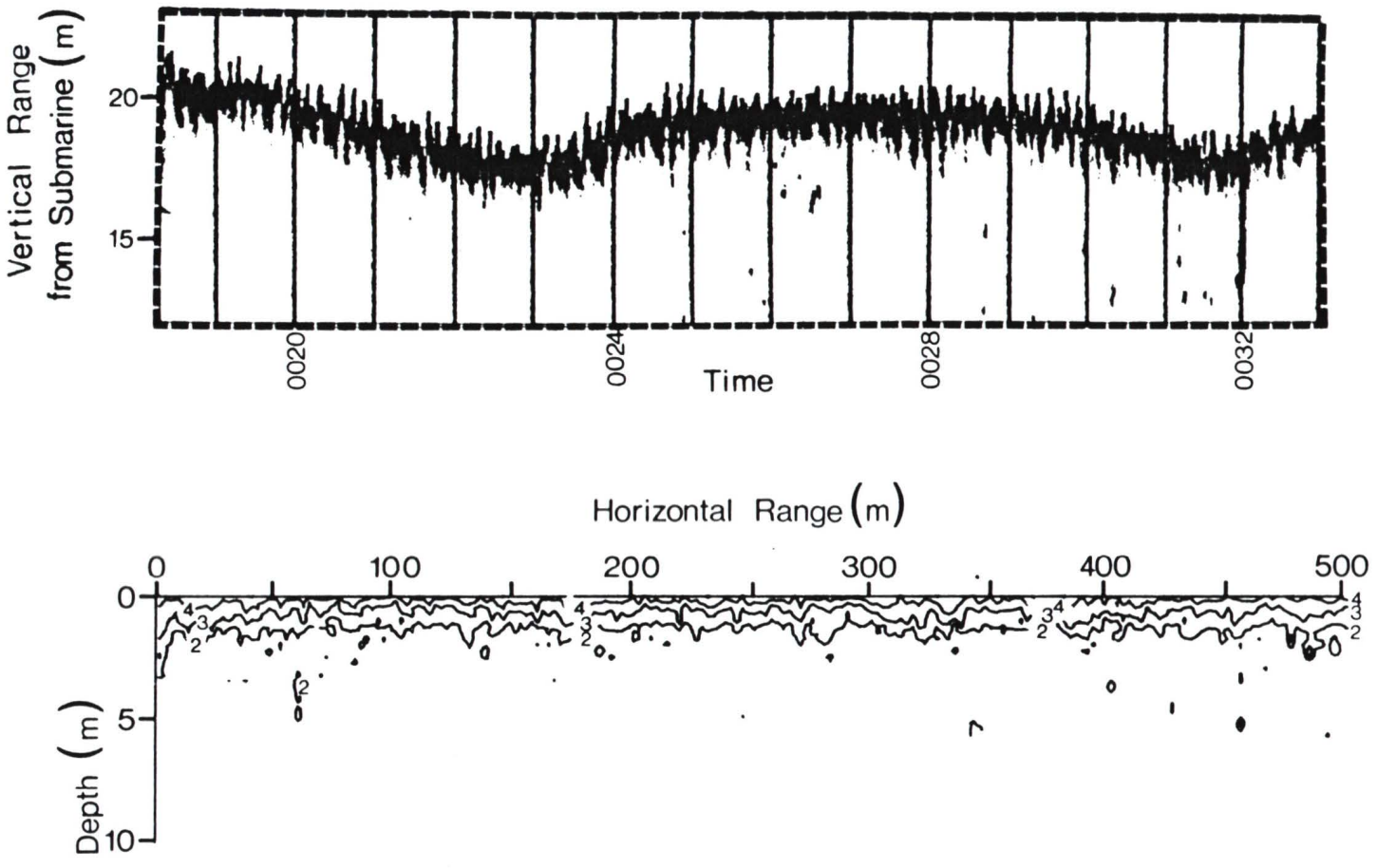

Figure 19 - Observations of the distribution of bubbles: (a) an acoustic backscatter image; (b) contour plot of the (logarithm of the) bubble concentration as a function of horizontal range and of depth (October 10; $U_{10}=9ms^{-1}$ (uncertain); $\theta=45^{o}$; $\Delta T=-1^{o}C$; precipitation observed).

bubble densities (determined as indicated above). Note that the graphic images may not match the contours precisely, since the former are plotted against time and the latter aginst range. Winds were predominantly from the north-west for these observations, with a fetch effectively unlimited by land masses.

The data in figures 12 and 13 were collected at a wind speed of about $3ms^{-1}$ and show relatively few identifiable bubble clouds (ship speed information was not available for the latter set of data, so no corresponding spatial contours of bubbles are plotted). A scattering layer is present at about a meter below the surface in these two figures, but does not appear in other observations.

Figures 14 through 17 show bubbles produced at higher wind speeds under steady conditions. Bubble concentration is seen to increase as the wind increases. In addition, the depths to which bubbles penetrate also increases with wind speed. No bubble plumes were observed to penetrate to the depth of the main thermocline, which was nominally 20m below the surface. Figure 20 shows the mean and maximum depths to which bubbles penetrate before being lost in the background noise of the acoustic system and the ocean.

The shape of the bubble plumes in figure 15 are seen to be relatively columnar, while the majority of plumes in figure 14 are broader and more 'billow-like'. This is consistent with the

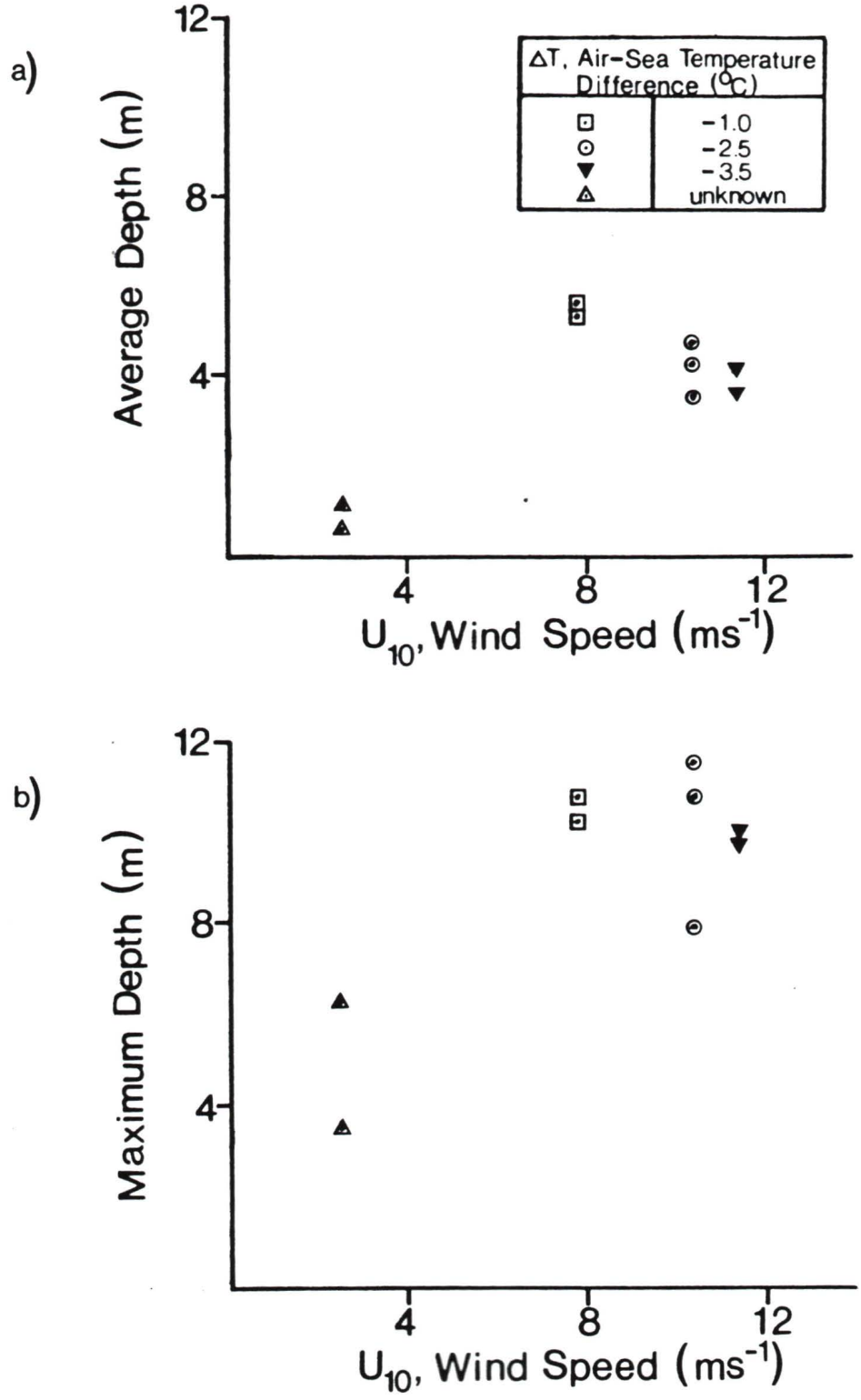

Figure 20 - Depths to which bubbles penetrate as a function of wind speed: (a) average depth; (b) maximum depth.

observations of Thorpe and Stubbs (1979), who found that bubble clouds tend to be more columnar in the presence of a more negative air-sea temperature difference ΔT.

During the period of time over which the data in figures 18 and 19 were taken, the wind was observed to rise and fall quickly and dramatically. In addition, rain was observed during collection of the data in figure 19. Bubble densities in figure 19 are significantly less than in figure 18. The distribution of bubbles in figure 19 is also very nearly uniform in the horizontal.

Power spectra of the (logarithm of the) bubble concentration were calculated at fixed depths in order to determine whether or not the bubble plumes show some regular spacing. The depths were chosen a few meters below the surface so as to avoid the fairly uniform near-surface layer of bubbles observed at higher wind speeds. In order to allow us to relate the spectral results to length scales, data selection was limited to measurements obtained at relatively fixed ship speeds. Power spectra are provided in figure 21 for four different cases. The forward ship speed was used to convert time scales to length scales.

The spectrum in figure 21a corresponds to the data in figure 19 at a depth of 2m. The submarine was travelling at about 45^{o} to the wind direction. The associated wind speed, as previously mentioned,

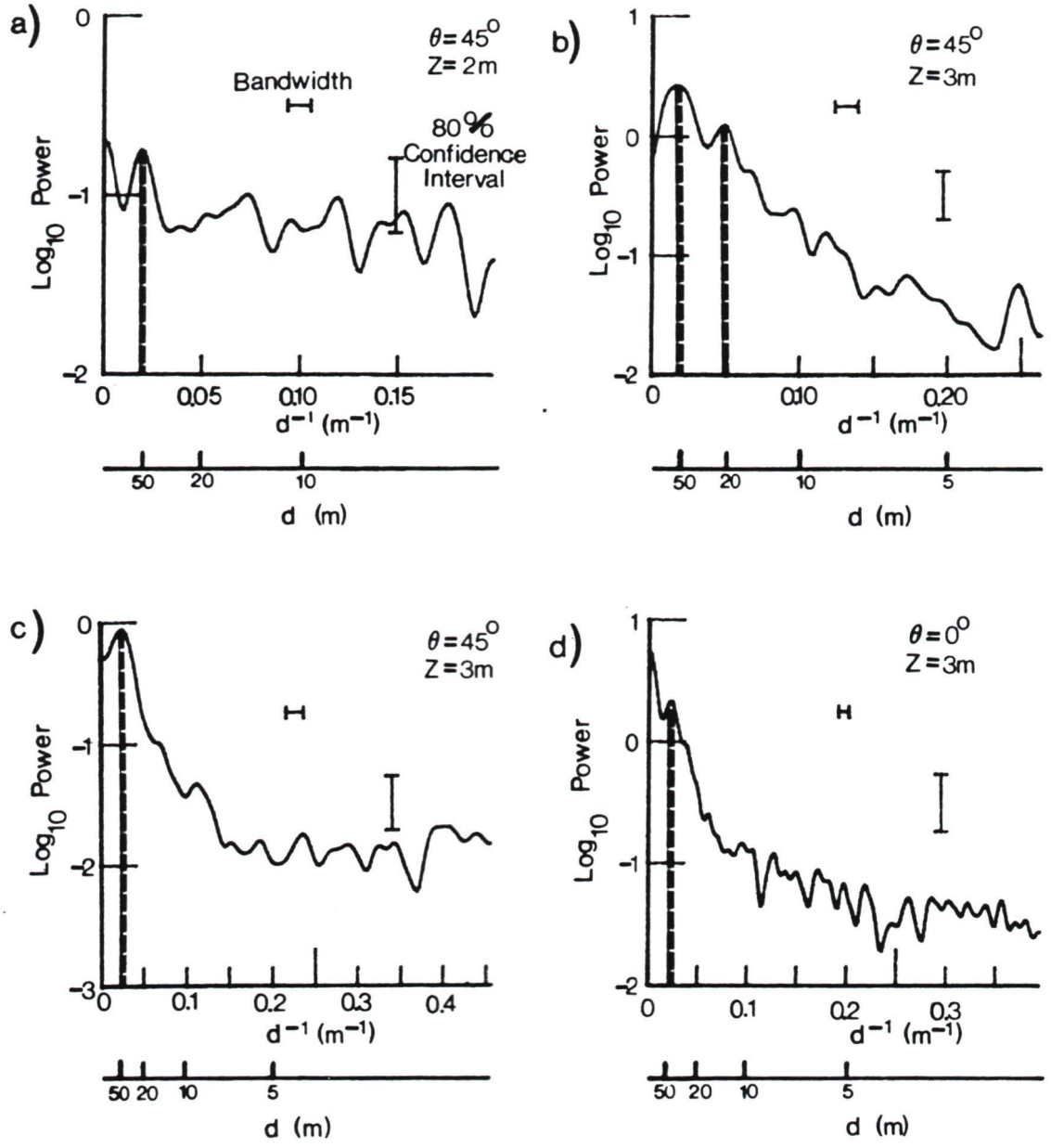

Figure 21 - Power spectra of the horizontal distribution of $\log_{10}(N)$ corresponding to the data depicted in: (a) figure 19 (a peak of interest occurs at about $0.019m^{-1}$); (b) figure 14 (peaks occur at about $0.017m^{-1}$ and $0.049m^{-1}$); (c) figure 13 (peak is located at about $0.025m^{-1}$); (d) figure 17 (with a small peak at about $0.022m^{-1}$). Power is in arbitrary units.

is uncertain. The dynamic range of results in the spectrum is not extensive, but there is a distinct peak at about $0.019m^{-1}$, corresponding to a length scale of about 53m (we shall ignore the peak at $0m^{-1}$).

Figure 21b corresponds to the observations at 3m depth shown in figure 14. These observations were made at 45^{o} to the wind direction and at a wind speed of $11ms^{-1}$. The dominant peak occurs at $0.017m^{-1}$ (or a length scale of about 59m) and a second peak at about $0.049m^{-1}$ (quite probably a third harmonic of the dominant peak). The data used to obtain the spectrum in figure 21c were collected at the same depth and correspond to the plots in figure 15. The wind speed in this latter case was about $8ms^{-1}$ and the boat was travelling at about 45^{o} to the wind direction. A clear peak is observed at about $0.025m^{-1}$, or 40m.

The spectrum plotted in figure 21d was determined from the data in figure 17, which was collected while travelling with the wind. The wind speed was about $10ms^{-1}$. Although the spectrum falls off rapidly as the inverse length scale d^{-1} increases, there is a peak at about $0.022m^{-1}$ (or 45m).

Chapter 5

Discussion

Waves seldom break at low wind speeds, so bubble injection is rare and random. The data in figures 12 and 13, collected at a wind speed of 2-3ms^{-1}, show few identifiable bubble clouds, as one would expect. Just below the surface, however, is a distinct scattering layer which follows the surface variations very closely. The layer is probably a temporary thermocline (i.e. a strong temperature gradient) set up by the diurnal heating of the surface. Little wind forcing is present, so little turbulence is generated to mix the upper waters. Consequently, the daily cycle of heat exchange between the ocean and atmosphere is restricted to a region very close to the surface and a small thermocline may be created. The acoustic backscatter from the layer may be due to the thermocline itself or to biological targets resting on it.

In calculations of bubble concentrations, no attempt has been made to remove the effect of the near-surface scattering layer. It can, however, be easily identified in the contour plot in figure 12b. We shall use some caution in interpreting mean bubble populations in the presence of this acoustic target.

Several of the graphic images in figures 12 through 19 show

quite random, diffuse levels of backscatter at the base of some of the cloud-like structures (these diffuse features do not appear in the contour plots because of averaging within bins), while in other clouds much more dramatic transitions are observed at the outer edges of the clouds. This is particularly obvious in figure 14a. The random features occur in part because the bubbles are randomly positioned with respect to one another: the signal received by the transducer from any single transmission pulse is the sum of many signals scattered from individual bubbles, each with a random phase lag associated with the associated acoustic path. However, some of the variability may also be indicative of small-scale structures of bubbles. One might expect the more random, diffuse sections to be due to 'older' bubbles, which have been in the presence of turbulence longer and are therefore more randomly distributed than the more recently-injected bubbles.

Some bubble plumes appear somewhat 'slanted' in the water column, as in figure 14a. This occurs because of the current shear in the upper ocean, which strains the bubble clouds. The slope of these clouds can also give an indication of the relative age of the clouds. Older clouds will appear more stretched than more recent ones because they will have been subjected to the shear for a longer period of time. The slope of the clouds is obviously related to the amount of current shear in the upper ocean, the degree of turbulence

(which determines how deep the bubbles will go and how fast they reach that depth) and the length of time since the bubbles were entrained.

The wind speed associated with the bubble observations in figures 16 and 17 is quite similar to that associated with the data in figure 15. The depths to which the bubble clouds penetrate are similar, too, but the horizontal extents of the clouds are somewhat different. Thorpe and Hall (1983) have suggested that the initial dimensions of bubble clouds are determined by the duration of wave-breaking and the wave speed (which define the length of the cloud in the wind direction) and the length of the wave crest over which breaking occurs (which defines the cloud width). They found in general a ratio of cloud length to width of about 1.4, but noted that this value may increase somewhat in the presence of large near-surface current shear.

Observations of breaking waves were not available during the October DOLPHIN cruise, but we might surmise that surface conditions corresponding to the data in figures 15-17 were similar. The latter two data sets were collected while the submarine was running anti-parallel and parallel to the wind and the waves respectively, while the former data set was collected at about 45^{o} to the wind direction. Following the reasoning of Thorpe and Hall (1983), this might suggest a somewhat smaller ratio of cloud length to width than

1.4. Where individual plumes can be distinguished in figure 15, the horizontal extents all appear to be of the order of 5-10m; in figures 16 and 17, they appear to be of the order of 5-15m (we have taken into account in these estimates a broadening of the cloud images by about 5m due to the finite beam width). The ratio of horizontal extents of the bubble clouds (as measured parallel to and 45^{o} to the wind direction, respectively) is therefore between about 1.0 and 1.5. This is reasonably consistent with Thorpe and Hall's observations.

The wind event that occurred during collection of the data in figures 18 and 19 appears to have been short-lived. The lack of resolution in the atmospheric observations makes it difficult to interpret the exact conditions under which these data were collected. Linear interpolation between the atmospheric data samples suggests a wind speed of about $7ms^{-1}$ for figure 18, although one would not want to take this value too seriously without more accurate wind observations. The bubble plumes penetrate only to a depth of a few meters at most.

Bubble populations in figure 19 are significantly less than in figure 18. The atmospheric data suggests a wind speed of about $9ms^{-1}$, but this does not seem consistent with the bubble observations. Since the weather observations were made some 10km away from the site of the bubble observations, there was doubtless some time lag in the wind speed measurements. The high winds that were observed were

short-lived and appeared to rise and fall quickly.

The presence of rain can serve to quell wave motion (Manton 1973). Thorpe and Hall (1983) found that wave-breaking was substantially reduced in rainy conditions. This may have also contributed to the drastic difference in the sub-surface concentration of bubbles observed in figure 19 as compared with that in figure 18. Rain can also entrain bubbles. Thorpe and Hall noted that the input of bubbles by rain over the sea surface is much more uniform than the input by breaking waves. This is certainly consistent with the observations in figure 19b, where the bubbles are seen to be distributed relatively uniformly in the horizontal.

Figure 22 provides mean estimates of N as a function of depth under three different sets of wind conditions. At the lowest wind speed (about $3ms^{-1}$), waves break very infrequently and bubbles are entrained only to depths of a meter or so. At higher wind speeds, waves break more often and many more bubbles are entrained to greater depths. The population estimates below a depth of about 2m at the lowest wind speed are an indication of the background volume reverberation level, primarily due to the presence of biological scatterers near the surface, rather than actual bubbles. The background level varied significantly from dive to dive because of the diurnal vertical migration of plankton and their predators.

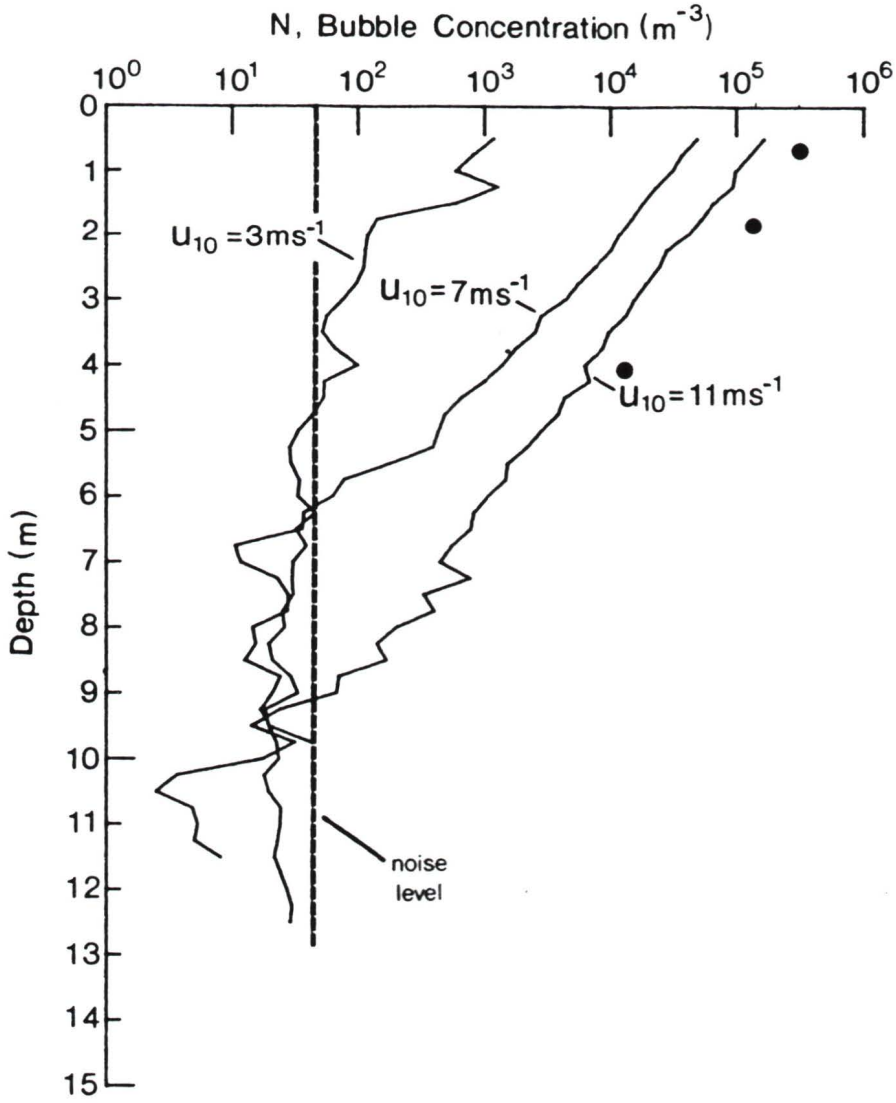

Figure 22 - Mean bubble concentration profiles at three different wind speeds. Observations by Johnson and Cooke at wind speeds of 11-13ms^{-1}, indicated by the black circles, are provided for comparison.

The effect of the near-surface scattering layer on bubble density estimates is seen at a depth of about 1.25m in the profile for the lowest wind velocity. This layer may lead to misinterpretation of the bubble distribution, but there does appear to be a net increase in the scattering levels irrespective of the presence of the layer. It is therefore appropriate to presume that much of the mean acoustic backscatter observed for this data set was due to bubbles.

Results obtained by Johnson and Cooke are also plotted in figure 22. The wind conditions were similar to those present for the profile corresponding to $11ms^{-1}$. Their results are of the same order of magnitude as our estimates, but ours are slightly lower. This is perhaps due to an inadequate model of the probability distribution, differences in atmospheric and oceanic conditions between the two sets of experiments or to measurement techniques. On the other hand, Thorpe (1984c) has suggested that in the presence of Langmuir circulation, the instrument used by Johnson and Cooke to make bubble measurements would be swept preferentially into regions of convergence, where anomalously large estimates of mean bubble density would be made. It is expected that over-estimates of N would be most significant near the surface. The results in figure 21 are consistent with this interpretation. In any case, it is significant that measurements of the mean bubble density obtained using the

acoustic system are comparable to the measurements of Johnson and Cooke.

It is interesting that our acoustic measurements of mean bubble density and those implied by Thorpe (1982) are quite consistent with the direct measurements of Johnson and Cooke (1979), while the acoustic studies of Medwin (1970,1977a) and Dalen and Lovik (1981) suggest much higher bubble concentrations under similar conditions. The reason for this dichotomy is not clear. However, we note that Thorpe's observations as well as our own were made using upward-pointing acoustic systems located well below the ocean surface and the bubbles. Those observations made by Medwin and by Dalen and Lovik were made using downward-looking systems positioned near the surface, amidst the highest concentrations of bubbles. The two latter studies would be more easily subject to interactions between the instruments and the dynamic near-surface environment and to multiple scattering effects than the former ones.

The profiles in figure 22 indicate an exponential decrease in the mean bubble concentration with depth. This is consistent with the observations of Johnson and Cooke (1979) and with measurements of S_s (which was assumed proportional to the total number of bubbles) by Thorpe(1982). Estimates of the e-folding depth z_e (i.e. the change in depth required for the bubble density to change by a factor of e^{-1}) and the bubble concentration at the surface N_o were determined by a

least squares fit of the mean profiles to a function of the form $N_o \exp(-z/z_e)$. The fits were performed down to the depth at which the mean profiles reached the background noise level.

Figure 23 indicates estimates of N_o at different wind speeds. The distribution of points is poor, the data being clustered in two regimes. However, since the bubbles are generated at the surface by breaking wind waves, it is reasonable to presume that N_o is predominantly a function of wind speed. A least squares fit to the data indicates that N_o increases with wind speed roughly as $N_o \sim U_{10}^{3.0 \pm 0.3}$, where U_{10} is the wind speed measured 10m above the surface. This is consistent with a theory relating N_o to the rate of work done on the surface by the wind (Crowther 1980), which predicts a cubic dependence. Crowther (1980, 1985) has provided acoustic backscatter strengths which support this premise. Crowther (1985) has also analyzed some of Thorpe's (1982) observations and found the scattering cross-section, extrapolated to the surface, goes roughly as $S_s \sim U_{10}^{2.9}$ down to a wind speed of $3 ms^{-1}$. Farmer and Lemon (1984) evaluated bubble populations as a function of wind speed using a model of attenuation of wind-generated noise by bubbles, and found the slope to be just less than 3 for moderate winds. This is in contrast to results obtained by Wu (1981) who, in an analysis of data collected by Johnson and Cooke (1979) and Kolovayev (1976), suggested $N_o \sim U_{10}^{4.5}$.

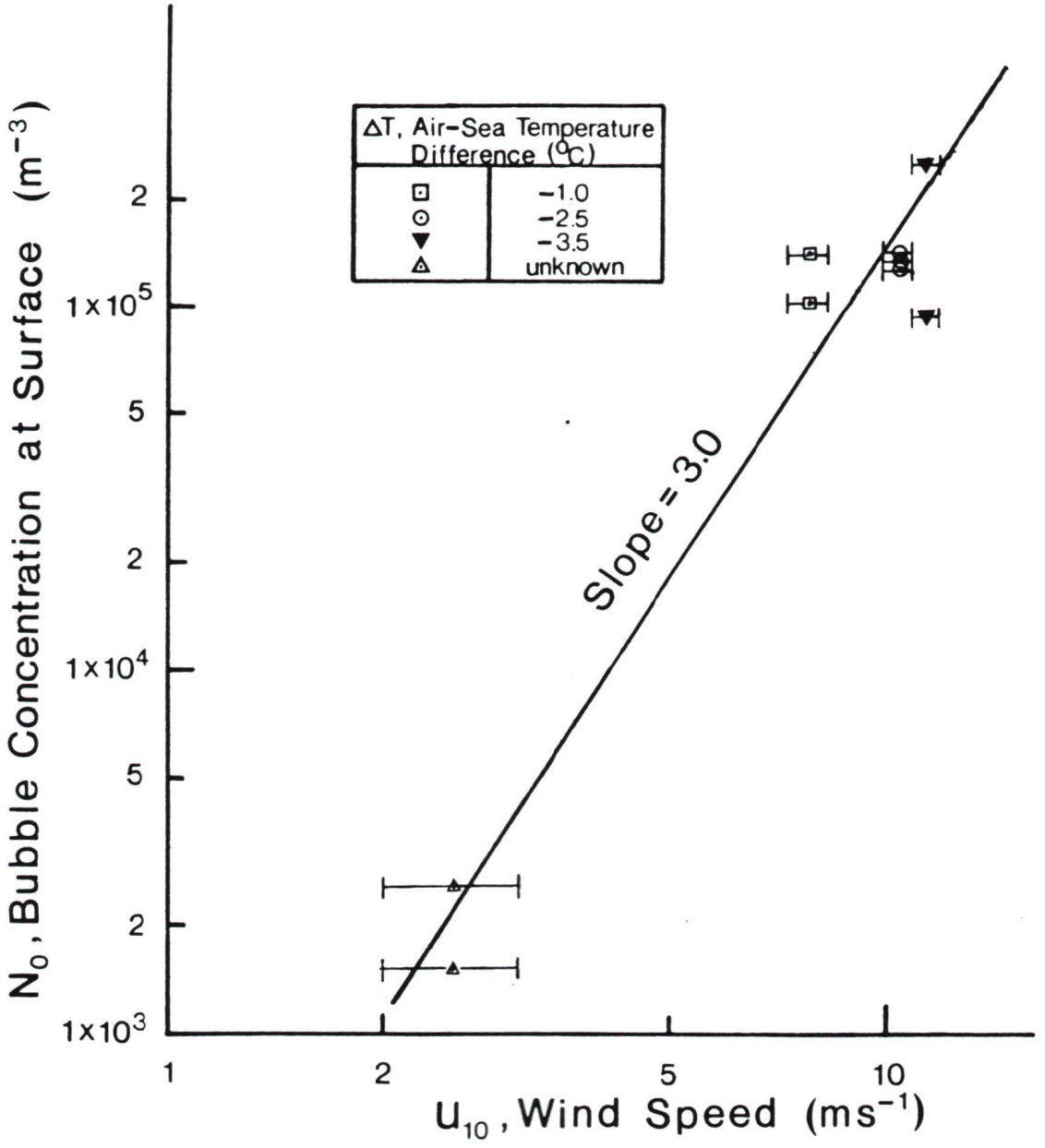

Figure 23 - Estimates of the mean bubble concentration at the surface as a function of wind speed.

Values of z_e were seen to vary between 0.7m and 1.5m. The values are plotted against wind speed in figure 24a. There is a general increase with wind speed, but there is also much variability. This is at least partly due to differences in the level of convective turbulence associated with the air-sea temperature gradient, which contributes to the net turbulence and hence influences the depths to which bubbles penetrate. Thus one would not expect the e-folding depth to be a function of wind speed only.

Figure 24b shows a plot of the average number of bubbles below the surface per unit area of the ocean surface, N_T. These estimates were made by integrating the function $N_o \exp(-z/z_e)$ down to the mean depth at which the backscatter reached noise level. The values used for N_o and z_e were those obtained from the least squares fit previously described. Since z_e was never very large (~1m) and did not vary by more than a factor of about 2, the values of N_T were dominated by the values of N_o.

The mean volume of bubbles below the surface per unit area of the ocean surface, V_T, is also shown in figure 24b. Under the assumed size distribution of bubbles (equation (4.9)), V_T is proportional to N_T, where the constant of proportionality is given by

$$\varepsilon = \int_0^\infty \frac{4}{3} \pi a^3 \, p(a) \, da \, . \qquad (5.1)$$

This integral was evaluated analytically to be about $9.7 \times 10^{-13} m^3$.

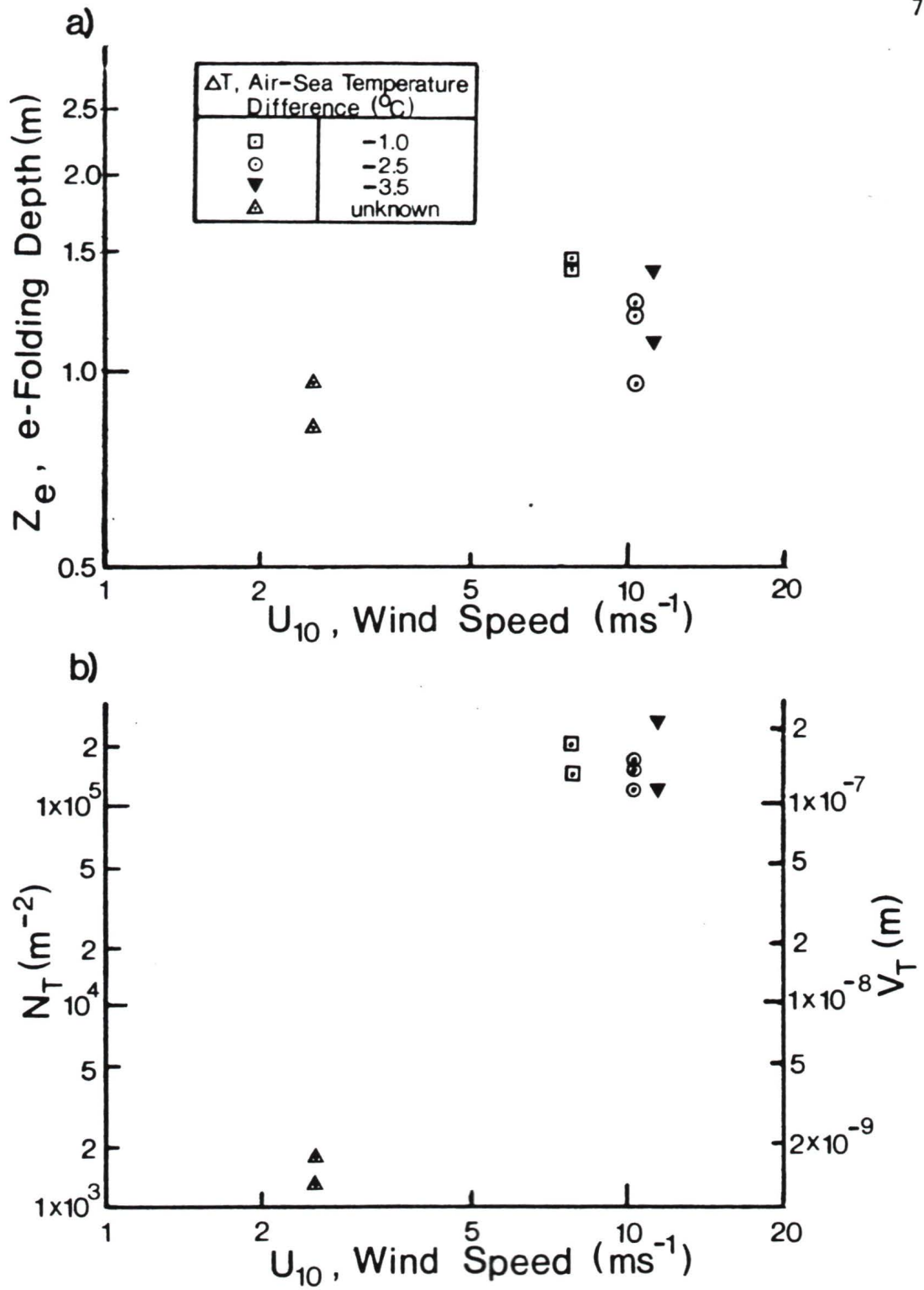

Figure 24 - (a) Variation of the e-folding depth as a function of wind speed. (b) Estimates of the mean number and mean volume of bubbles below the surface per unit area of the surface as a function of wind speed.

The reason for the exponential dependence of N on depth is still not completely understood. However, a number of models of bubble dynamics have been developed which shed light on the problem. Crowther (1980) developed a simple vertical diffusion model of bubble transport (neglecting the effects of hydrostatic compression and gas diffusion on the bubbles) which is given by the equation

$$\frac{\partial n}{\partial t} - K\frac{\partial^2 n}{\partial z^2} - W_b\frac{\partial n}{\partial z} = S\,\delta(z) \qquad (5.2)$$

where t is time, S is the source function for the bubbles at the surface, δ is the Dirac delta function, K is a diffusion coefficient (assumed constant) and W_b is the terminal velocity of a bubble of radius a. This equation has a steady-state solution of the form

$$n(a) \propto \frac{S(a)}{W_b(a)}\exp(-W_b z/K). \qquad (5.3)$$

Crowther suggested that the source function should be proportional to the rate of work done on the surface. He used a dimensional argument to propose a source function of the form

$$S(a) \propto U^3/\tau a^3 \qquad (5.4)$$

where U is the wind speed and τ is the kinematic surface tension.

Thorpe (1982,1984b,c) has modelled bubble dynamics in more detail using a steady-state equation of the form

$$K\frac{d^2n}{dz^2} + \left(\frac{dK}{dz} + W_b\right)\frac{dn}{dz} - \phi(a,z,h)\frac{dn}{da} = 0 \quad (5.5)$$

where K=K(z), h is the gas saturation, and ϕ is a complicated function which takes into account bubble contraction or expansion due to gas diffusion across the bubble surface and to hydrostatic pressure. Thorpe has used various expressions for ϕ and has modelled analytically and numerically. the steady-state distribution of bubbles for K constant and for K proportional to depth.

Crowther (1985) has recently used Thorpe's (1984b) model, neglecting ϕ, with a diffusion coefficient of the form

$$K = K_o \exp(-\beta z) \quad (5.6)$$

and has obtained an analytical solution for the distribution of bubbles of the form

$$n(a,z) = n_o(a)\ \frac{\exp[(q\exp(-\beta z)) - 1]}{\exp(q) - 1} \quad (5.7)$$

where $n_o(a)$ is the concentration of bubbles at the surface with radii between a and a+da, β is a constant and

$$q = W_b / \beta K_o \ . \quad (5.8)$$

For small bubbles, this gives

$$n \propto \exp(-\beta z) \quad (5.9)$$

and for large bubbles

$$n \propto \exp(-W_b z/K) . \qquad (5.10)$$

Thus, the variation in bubble concentration n with depth is independent of bubble size for small bubbles. Most observations of bubble spectra indicate the majority of bubbles lie within a narrow band of radii (of the order of 20-80μm), so one might expect the total concentration of bubbles N to follow a similar type of exponential dependence.

The aforementioned models are based on statistically steady conditions, but the input of bubbles by breaking waves is far from being uniform and continuous. The contours of bubble concentration in figures 15-19 show nearly uniform vertical spacing for the most part, although the spacing is seen to change with horizontal range. This suggests that an exponential decrease in bubble concentration with depth is present throughout most of the bubble distribution. The differences in the e-folding depth may reflect variations in the local turbulence levels.

Figure 25 shows two bubble population profiles, averaged over roughly 10-minute periods and many bubble clouds for a wind speed of $10 ms^{-1}$. The two data sets were collected about 2 hours apart. The e-folding scale is observed to be quite different, as indicated by the different profile slopes. Mean bubble density estimates at 4m depth are seen to vary by a factor of nearly 4. Bubble densities

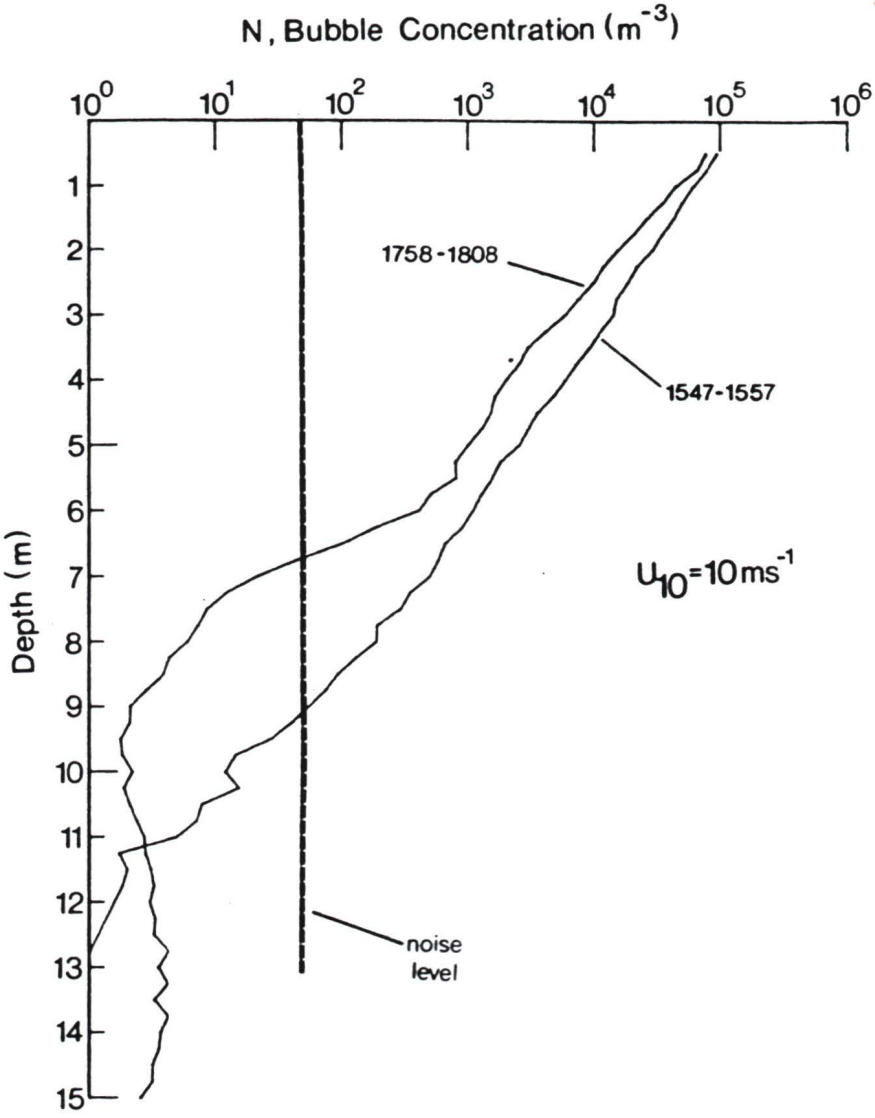

Figure 25 - Two mean bubble concentration profiles determined from data collected at the same wind speed on October 17, 1984. The concentrations are similar near the surface, but decrease with depth at different rates. These differences may be due to differences in the average level of turbulence between the two data sets.

extrapolated to the surface, however, are quite similar for the profiles shown. Thus the bubble concentration at the surface was fairly constant. Following Crowther (1980), this implies the wind forcing was also constant, which agrees with the meteorological measurement. This suggests that the mean turbulence level near the surface, which determines the depths to which bubbles are transported, can vary significantly in space-time under conditions of (presumably) constant wind forcing. Such a result provides an alternative explanation for the differences between bubble populations observed by Johnson and Cooke (1979) and our measurements. Variations in average turbulence levels will influence the mean bubble density at a given depth.

Are the bubble plumes directly related to individual breaking events on the ocean surface? Much of the recent literature on bubbles has suggested or implied this (as we have done), and indeed the hypothesis does not seem to be an unreasonable one. Favourable evidence has been building (e.g. Thorpe and Humphries 1980; Thorpe and Hall 1983), but the hypothesis has not been proved.

The spacing between bubble plumes may give further insight to this question. Unfortunately, no surface observations were made during the field experiments, so we are unable to compare directly our bubble observations to the spacing between breaking waves. Furthermore, few studies of the scales of breaking events appear in

the literature. Most of these have been limited to the percentage of whitecap coverage of the surface (e.g. Monahan and Muircheartaigh 1980). Donelan et al (1972) have observed the appearance of whitecaps within a given wave group to occur with a period of about twice the period of the dominant (presumably locally-forced) waves. They have attributed this to the difference between the phase velocity and the group velocity (which is very nearly half the phase velocity for deep water waves). Thorpe and Humphries (1980) have found similar results in a lake. As previously mentioned, Thorpe and Hall (1983) have indicated that the ratio of bubble cloud length to width (both measured in the horizontal plane) is similar to that of the foam patches on the surface associated with breaking waves. They have also found that bubble clouds typically last for about 1 minute.

Ochi and Tsai (1983) have studied the predictability of wave-breaking using a criterion based on the observed wave height and period. A recent set of papers (Snyder and Kennedy 1983; Kennedy and Snyder 1983; Snyder et al 1983) discuss a wave-breaking criterion based on the vertical acceleration of the ocean surface and present geometrical and statistical results from a model and a field study. Longuet-Higgins and Smith (1983) and Weissman et al (1984) have also recently reported field observations of breaking events.

Let us presume the bubble plumes are generated by whitecapping on the surface. Let us further assume the peak frequency f_p

associated with the locally-forced wave spectrum is that frequency corresponding to the waves that break. We would expect a random occurrence of the conditions required for wave-breaking at any given location. However, once breaking does occur, one would expect to see periodic breaking in the downwind direction with a period of about $2T_p$ and corresponding spatial separation $2\lambda_p$, where $T_p=f_p^{-1}$ and λ_p is the associated wavelength (from equation (4.1)). In other words, one would expect no regular spacing between bubble plumes, except in the downwind direction. In this latter case, plumes generated by the same wave group will be correlated.

Of course, we cannot ignore the 'lifetime' of the bubbles in this simple picture. Bubble plumes are not permanent fixtures in the ocean. Following Thorpe and Hall (1983), we shall assume the bubble plumes last for about 1 minute.

If Langmuir circulation plays an important role in the formation of bubble plumes then we might expect to see somewhat regular spacing of plumes when travelling at angles to the wind direction. If the rate of bubble generation by breaking waves is high, then the Langmuir cells may be identified with long, horizontal collections of bubbles. If the input of bubbles by breaking waves is relatively infrequent (as observed at low wind speeds, when wave breaking seldom occurs), then the bubble plumes will be discrete entities, although they may still be shaped by the Langmuir flow.

In using these simple ideas to explain our observations, we need to be able to determine the peak frequency of the wave spectrum. A number of models of wave spectra exist (e.g. Hasselmann et al 1976), but these are restricted to fetch-limited conditions. As previously mentioned, the fetch was essentially unlimited for our data. However, Toba (1973) has indicated that the dominant frequency of a wind-wave spectrum can be determined from the significant wave period $T_{1/3}$ by the equation

$$f_p = (1.05\, T_{1/3})^{-1} \quad . \qquad (5.11)$$

We therefore resort to deep water forecasting curves (U.S. Army Coastal Research Center 1984), which allow estimation of $T_{1/3}$ from wind speed and duration.

For the data in figure 21d, the wind had been blowing at about $10ms^{-1}$ for between 3 and 6 hours, giving a significant wave period of between 3.8s and 4.6s. The frequency of the dominant wave was then (from equation (5.11)) between 0.22Hz and 0.26Hz and the expected spacing $2\lambda_p$ between whitecap events (from equation (4.1))was between 45m and 66m. The spacing between bubble plumes, as implied from the spectral peak in figure 21d, was about 45m, which is within the (albeit wide) range of expected spacing between breaking events on the surface. This provides further evidence that bubble plumes are generated by breaking waves.

The phase speed of the breaking surface waves was between about $5.9ms^{-1}$ and $7.2ms^{-1}$ and the submarine was moving downwind at a speed of about $1.3ms^{-1}$ for this data set. If we assume the bubble plumes last for about a minute, then we would see at most 2-3 bubble plumes generated by the same wave group. In the meantime, other groups of breaking waves may have passed overhead and entrained bubbles. Thus, at this relatively low ship speed, we would not expect to see a truly periodic signal in the horizontal distribution of bubbles, but at best might hope to observe a small spectral peak associated with the spacing between bubble plumes. The peak in figure 21d is consistent with this interpretation.

Data collected at an angle to the wind direction also showed some regular spacing. If we presume the observed bubble cloud distribution is a manifestation of Langmuir circulation (i.e. long, horizontal rows of bubbles aligned in the wind direction), then the inferred spacing between wind rows is the projection of the observed spacing of bubble plumes along a horizontal vector perpendicular to the wind direction. The implied wind row spacings from figures 25a, b and c are about 37m, 42m and 28m, respectively. These results are not inconsistent with observations of wind row spacings in the ocean. For example, at a wind speed of $5\text{-}8ms^{-1}$, Katz et al (1965) found row spacings between 10m and 30m; at a wind speed of about $10ms^{-1}$, Assaf et al (1971) observed a separation between the dominant

wind rows of about 44m. No one has yet been able to parameterize the spacing between wind rows in the ocean.

These observations would seem to suggest that Langmuir circulation plays an important role in the distribution of bubbles below the surface. On the other hand, there is no extensive elongation of the bubble plumes in the downwind direction in figure 17. There is no indication of the existence of long, horizontal rows of bubbles aligned with the wind. Perhaps the flux of bubbles across the air-sea interface is insufficient to 'visualize' properly Langmuir cells, but this does not explain the presence of the spectral peaks in figures 21a, b and c. It is unlikely that the submarine would have been travelling down the middle of two wind rows while running with the wind, but this does provide an alternative explanation.

It appears that the dynamics affecting the localized distribution of bubbles may not be so simple as to be modelled accurately by simple one-dimensional or even two-dimensional models. The level of turbulence and the rate of generation and entrainment of bubbles play important roles in the distribution of bubbles; so may Langmuir circulation. Further research is required before we can assess the relative importance of these quantities. We need to be able to relate the spatial distribution of bubbles to simultaneous observations of Langmuir circulation (especially the spacing between

wind rows) and wave-breaking events as well as measurements of turbulence in the near-surface ocean.

Chapter 6

Conclusions

The purpose of the work reported in this thesis was to study the spatial distribution of bubbles generated by breaking waves. Observations of bubbles were obtained using an upward-pointing acoustic transducer mounted on the deck of the submarine USS DOLPHIN. Studies were carried out about 10km off the coast of Monterey, California during October 1984, under conditions of low-to-moderate wind speeds ($3\text{-}11 ms^{-1}$).

Previous acoustic studies of bubble concentration have been limited to presentation of scattering cross-section strengths (e.g. Thorpe 1982) or concentrations of bubbles of one size (e.g. Medwin 1977a). In addition, spatial distributions of bubbles have been resolved only in the vertical or horizontal. We present for the first time acoustic measurements of the total concentration of bubbles, N, inferred from a simple model of the bubble size spectrum. The results are also unique in that they represent two-dimensional profiles of the bubble concentration under different conditions, indicating both the horizontal and vertical dependence of N.

The wind is responsible for the generation of current shear and

waves. It is indirectly responsible for the input of bubbles and the level of mechanical turbulence and therefore influences strongly the distribution of bubbles. This was apparent in the observations presented in this thesis. At low wind speeds, few identifiable patches of bubbles were observed. At higher wind speeds, the bubble concentration increases. In addition, the depths to which bubbles penetrate also increase with wind. speed. As the wind speed increases, wave-breaking occurs more frequently and with greater force, entraining more bubbles and generating more turbulence. Consequently, bubbles are able to penetrate to greater depths in greater quantities.

Estimates of N were averaged horizontally to provide vertical profiles of the mean bubble concentration. The results are consistent with the results obtained by Johnson and Cooke (1979) under similar wind conditions. The profiles indicate an exponential dependence of the average value of N on depth, as observed by Johnson and Cooke (1979) and inferred by Thorpe (1982). The results are consistent with a simple one-dimensional model of bubble dynamics and distributions developed by Crowther (1980).

The bubble concentration at the surface N_o and the e-folding depth z_e were determined from a least squares fit of each of the average profiles of N to a function of the form $N_o \exp(-z/z_e)$. The mean number and volume of bubbles below the surface per unit area of

the surface, N_T and V_T respectively, were estimated by integrating the function $N_o \exp(-z/z_e)$ down to the mean depth at which the acoustic backscatter reached the noise level.

Although the distribution of data points was poor, a least squares fit of the estimates of N_o indicated that $N_o \sim U_{10}^{3.0 \pm 0.3}$, where U_{10} is the wind speed measured 10m above the surface. This is consistent with Crowther's (1980) diffusion model, relating N_o to the rate of work done on the surface by the wind, and with observations presented by Crowther (1980, 1985) and Farmer and Lemon (1984).

A number of results presented in this thesis indicate that the wind speed is not the only parameter influencing the spatial distribution of bubbles. Estimates of z_e, N_T and V_T were found in general to increase with wind speed, but significant variability was also detected. This may well be due to differences in the level of convective turbulence, which contributes to the net turbulence in the upper ocean. The importance of convective turbulence, as inferred from the air-sea temperature difference, to the distribution of bubbles was also apparent from the shapes of the bubble plumes. The plumes were seen to be more columnar when ΔT was more negative, or when the level of convective turbulence was greater.

Evidence was obtained which indicates the bubble plumes are directly related to breaking events on the ocean surface. The

horizontal extents of bubble plumes, as measured in directions parallel and at 45^{o} to the wind direction under similar wind conditions and values of T, were determined. The ratio of the extents in the two different directions was found to be consistent with the ratio of the horizontal scales over which waves break, as suggested by Thorpe and Hall(1983). In addition, data collected while travelling in the downwind direction showed a spectral peak corresponding to a separation of bubble plumes of about 45m. This compared favourably with the expected spacing between breaking events.

An indication of fairly regular spacing between bubble plumes was also present in data sets collected at an angle to the wind direction. If the distribution of bubbles is dominated by Langmuir circulation, we might expect long, horizontal rows of bubbles aligned with the wind to be present. Under this assumption, the associated spacing between 'bubble rows' was determined for these data sets. The results were comparable to direct observations of wind row spacing by other researchers under similar wind conditions. On the other hand, there was no evidence of extensive elongation of bubble plumes in the downwind direction. We conclude that Langmuir circulation may play an important role in the distribution of bubbles, but we cannot identify its relative importance.

In summarizing the results in this thesis, a number of

recommendations for future bubble studies come to mind. Direct measurement of the wind speed and direction, the wave spectrum, the net heat flux, the turbulence and the wind row spacing (when present) would allow assessment of the relative importance of these parameters to the distribution of bubbles.

It would be very interesting to observe a bubble plume form under a breaking wave. This might be done with a narrow-beam transducer mounted below a freely-floating surface buoy, or with a steered array of transducers mounted on the sea floor in relatively shallow water. This latter arrangement would also make it possible to obtain a three-dimensional image of the distribution of bubbles.

Finally, doppler analysis of acoustic returns from an upward-pointing transducer would give information on the vertical velocities of bubbles (provided the acoustic system has a sufficiently small bandwidth and high frequency in order to resolve the relatively low speeds), which would help us to understand the forces responsible.

The interactions between the ocean and the atmosphere are complicated and difficult to investigate. Bubbles play very important roles in many of these interactions, including gas exchange and the propagation of underwater sound. Acoustic studies of bubbles can provide much information on the fluid dynamics and gas levels in

the upper ocean, as well as the underlying physical processes involved.

References

Aleksandrov, A.P. and E.S. Vaindruk, 1974. Measurement of the parameters of an aerated sea layer as a method of remote investigation of near-surface vertical turbulence. The Investigation of the Variability of Hydrophysical Fields in the Ocean, R. Ozmidov, ed., Nauka Publishing, Moscow, 122-128.

Assaf, G., R. Gerard and A. L. Gordon, 1971. Some mechanisms of oceanic mixing revealed in aerial photographs. J. Geophys. Res., vol. 76, 6550-6572.

Blanchard, D.C., 1963. The electrification of atmosphere by particles from bubbles in the sea. Prog. Oceanogr., vol. 1, 71-202.

Blanchard, D.C. and L.D. Syzdik, 1972. Concentration of bacteria in jet drops from bursting bubbles. J. Geophys. Res., vol. 77, 5087-5099.

Blanchard, D.C. and L.D. Syzdik, 1974. Importance of bubble scavenging in the water-to-air transfer of organic material and bacteria. J. de Rech. Atmos., vol. 8, 529-540.

Blanchard, D.C. and A.H. Woodcock, 1957. Bubble formation and modification in the sea and its meteorological significance. Tellus, 1957, vol. 9, 145-158.

Broecker, H.C. and W. Siems, 1984. The role of bubbles for gas transfer from water to air at higher wind speeds. Experiments in the wind-wave facility in Hamburg. Gas Transfer at Water Interfaces, W. Brutsaert and G.H. Jirka, eds. D. Reidel Publishing, Dordrecht, Holland, 229-236.

Chapelon, J.Y., P.M. Shankar and V.L. Newhouse, 1985. Ultrasonic measurement of bubble cloud size profiles. J. Acoust. Soc. Amer., vol. 78, 196-201.

Clay, C.S. and H. Medwin, 1977. Acoustical Oceanography: Principles and Applications. Wiley, New York.

Cokelet, E.D., 1977. Breaking waves. Nature, vol. 267, 769-774.

Craik, A.D.D., 1977. The generation of Langmuir circulations by an instability mechanism. J. Fluid Mech., vol. 81, 209-223.

Craik, A.D.D. and S. Leobovich, 1976. A rational model for Langmuir circulations. J. Fluid Mech., vol. 73, 401-426.

Crowther, P.A., 1980. Acoustical scattering from near-surface bubble layers. Cavitation and Inhomogeneities in Underwater Acoustics, W. Lauterborn, ed. Springer-Verlag, Berlin, 194-204.

Crowther, P.A., 1985. Modelling of sea surface scattering. Proc. Inst. Acoustics, vol. 7, 49-57.

Dalen, J. and A. Lovik, 1981. The influence of wind-induced bubbles on echo integration surveys. J. Acoust. Soc. Amer., vol. 69, 1653-1659.

Devin, C., Jr., 1959. Survey of thermal, radiation and viscous damping of pulsating bubbles. J. Acoust. Soc. Amer., vol. 31., 1654-1667.

Dillon, T.M. and D.R. Caldwell, 1980. The Batchelor spectrum and dissipation in the upper ocean. J. Geophys. Res., vol. 85, C4, 1910-1916.

Donelan, M.A., 1978. Whitecaps and momentum transfer. Turbulent Fluxes Through the Sea Surface, Wave Dynamics and Prediction, A. Favre and K. Hasselmann, eds. Plenum Press, New York.

Donelan, M.A., Longuet-Higgins, M.S., and J.S. Turner, 1972. Periodicity in whitecaps. Nature, vol. 239, 449-451.

Duce, R.A. and E.J. Hoffman, 1976. Chemical fractionation at the air-sea interface. Ann. Rev. Earth Planet. Sci., vol. 4, 187-228.

Eller, A.I., 1970. Damping constants of pulsating bubbles. J. Acoust. Soc. Amer., vol. 47, 1469-1470.

Faller, A.J. and C. Perini, 1984. The roles of Langmuir circulations in gas transfer across natural water surfaces. Gas Transfer at Water Surfaces, W. Brutsaert and G.H. Jirka, eds. D. Reidel, Dordrecht, Holland, 191-199.

Farmer, D.M. and D.D. Lemon, 1984. The influence of bubbles on ambient noise in the ocean at high wind speeds. J. Phys. Oceanogr., vol. 14, 1762-1778.

Garrett, C.J.R., 1976. Generation of Langmuir circulations by surface waves - a feedback mechanism. J. Mar. Res., vol. 34, 117-130.

Garrettson, G.A., 1973. Bubble transport theory with application to the upper ocean. J. Fluid Mech., vol. 59, 187-206.

Gill, A.E., 1982. Atmosphere-Ocean Dynamics. Academic Press, New York.

Glazman, R.E., 1983. Effects of adsorbed films on gas bubble radial oscillations. J. Acoust. Soc. Amer., vol. 74, 980-986.

Glazman, R.E., 1984. Damping of bubble oscillations induced by transport of surfactants between the adsorbed film and the bulk solution. J. Acoust. Soc. Amer., vol. 76, 890-896.

Glotov, V.P., P.A. Kolobaev and G.G. Neuimin, 1962. Investigation of scattering of sound by bubbles generated by an artifical wind in sea water and the statistical distribution of bubble sizes. Sov. Phys. Acoust., vol. 7, 341-345.

Hasselmann, K., D.B. Ross, P Muller and W. Sell, 1976. A parametric wave prediction model. J. Phys. Oceanogr., vol. 6, 200-228.

Holliday, D.V. and R.E. Pieper, 1980. Volume scattering strengths and zooplankton distributions at acoustic frequencies between 0.5 and 3 MHz. J. Acoust. Soc. Amer., vol. 67, 135-146.

Hsu, Y.L., P.A. Hwang and J. Wu, 1984. Bubbles produced by breaking wind waves. Gas Transfer at Water Surfaces, W. Brutsaert and G.H. Jirka, eds. D. Riedel, Dordrecht, Holland, 221-227.

Johnson, B.C. and R.C. Cooke, 1979. Bubble population and spectra in coastal waters: a photographic approach. J. Geophys. Res., vol. 84, 3761-3766.

Kanwisher, J., 1963. On the exchange of gases between the atmosphere and the sea. Deep-Sea Res., vol. 10, 195-207.

Katz, B., R. Gerard, and M. Costin, 1965. Responses of dye tracers to sea surface conditions. J. Geophys. Res., vol. 70, 5505-5513.

Kennedy, R.M. and R.L. Snyder, 1983. On the formation of whitecaps by a threshold mechanism. Part II: Monte Carlo experiments. J. Phys. Oceanogr., vol. 13 , 1493-1504.

Kerman, B.R., 1982. Distribution of bubbles near the ocean surface. Report AQRB-82-008-1, Atmospheric Environment Service, Canada.

Kinsman, B., 1965. Wind Waves. Prentice-Hall, Englewood Cliffs.

Kitaigorodskii, S.A., 1984. On the fluid dynamical theory of turbulent gas transfer across an air-sea interface in the presence of breaking waves. J. Phys. Oceanogr., vol. 14, 960-971.

Kolovayev, D.A., 1976. Investigation of the concentration and statistical size distribution of wind-produced bubbles in the near surface ocean. Oceanol., vol. 15, 659-661.

Lamb, H., 1932. Hydrodynamics, 6th edition. Cambridge University Press, New York.

Langmuir, I., 1938. Surface motion of water induced by wind. Science, vol. 87, 119-123.

Leobovich, S., 1983. The form and dynamics of Langmuir circulations. Ann. Rev. Fluid Mech., vol. 15, 391-427.

Longuet-Higgins, M.S. and N.D. Smith, 1983. Measurement of breaking waves by a surface jump meter. J. Geophys. Res., vol. 88, 9823-9831.

Ma, Y., V.K. Varadan and V.V. Varadan, 1983. Scattering of sound by gas bubbles in water and sediments. Presented at the 15th Annual Offshore Technology Conference, 525-532.

Manton, M., 1173. On the attenuation of sea waves by rain. Geophys. Fluid Dynamics, vol. 5, 249-260.

Medwin, H., 1970. In situ acoustic measurements of bubble populations in coastal ocean waters. J. Geophys. Res., vol. 75, 599-611.

Medwin, H., 1974. Sound phase and amplitude fluctuations due to temperature microstructure in the upper ocean. J. Acoust. Soc. Amer., vol. 56, 1105-1110.

Medwin, H., 1977a. In situ acoustic measurements of microbubbles at sea. J. Geophys. Res., vol. 82, C6, 971-976.

Medwin, H., 1977b. Counting bubbles acoustically: A review. Ultrasonics, vol. 15, 7-13.

Memery, L. and L. Merlivat, 1984. Contribution of bubbles to gas transfer across an air-water interface. Gas Transfer at Water Surfaces, W. Brutsaert and G.H. Jirka, eds. D. Reidel, Dordrecht, Holland, 247-253.

Monahan, E.C. and I.O. Muircheartaigh, 1980. Optimal power-law description of oceanic whitecap coverage dependence on wind speed. J. Phys. Oceanogr., vol. 10, 2094-2099.

Newhouse, V.L. and P.M. Shankar. Bubble size measurements using the nonlinear mixing of two frequencies. J. Acoust. Soc. Amer., vol. 75, 1473-1477.

Oakey, N.S., 1982. Determination of the rate of dissipation of turbulent energy from simultaneous temperature and velocity shear microstructure measurements. J. Phys. Oceanogr., vol. 12, 256-271.

Ochi, M.K. and C.H. Tsai, 1983. Prediction of occurrence of breaking waves in deep water. J. Phys. Oceanogr., vol. 13, 2008-2019.

Pond, S. and G.L. Pickard, 1983. Introductory Dynamical Oceanography. Pergamon Press, Oxford.

Shay, T.J. and M.C. Gregg, 1984. Turbulence in an oceanic convective mixed layer. Nature, vol. 310, 282-285.

Snyder, R.L. and R.M. Kennedy, 1983. On the formation of whitecaps by a threshold mechanism. Part I: Basic formulation. J. Phys. Oceanogr., vol. 13, 1483-1492.

Snyder, R.L., L. Smith and R.M. Kennedy, 1983. On the formation of whitecaps by a threshold mechanism. Part III: field experiment and comparison with theory. J. Phys. Oceanogr., vol. 13, 1505-1518.

Sutcliffe, W.H., Jr., E.R. Baylor and D.W. Menzel, 1963. Sea-surface chemistry and Langmuir circulation. Deep-Sea Res., vol. 10, 233-243.

Tennekes, H. and J.L. Lumley. A First Course in Turbulence. MIT Press, Cambridge, 1972.

Thomson, R.E., 1981. Oceanography of the British Columbia coast. Can Spec. Publ. Fish. Aquat. Sci. 56.

Thorpe, S.A., 1982. On the clouds of bubbles formed by breaking waves in deep water and their role in air-sea gas transfer. Phil. Trans. Roy. Soc. London, vol. A304, 155-210.

Thorpe, S.A., 1984a. The role of bubbles produced by breaking waves in super-saturating the near-surface ocean mixing layer with oxygen. Annales Geophysicae, vol. 2, 53-56.

Thorpe, S.A., 1984b. A model of the turbulent diffusion of bubbles below the sea surface. J. Phys. Oceanogr., vol. 14, 841-854.

Thorpe, S.A., 1984c. On the determination of K_v in the near-surface ocean from acoustic measurements of bubbles. J. Phys. Oceanogr., vol. 14, 855-863.

Thorpe, S.A., 1984d. The effect of Langmuir circulation on the distribution of submerged bubbles caused by breaking wind waves. J. Fluid Mech., vol. 142, 151-170.

Thorpe, S.A. and A.J. Hall, 1983. The characteristics of breaking waves, bubble clouds, and near-surface currents observed using side-scan sonar. Continental Shelf Res., vol. 1, 353-384.

Thorpe, S.A. and P.N. Humphries, 1980. Bubbles and breaking waves. Nature, vol. 283, 463-465.

Thorpe, S.A. and A.R. Stubbs, 1979. Bubbles in a freshwater lake. Nature, vol. 279, 403-405.

Thorpe, S.A., A.R. Stubbs, A.J. Hall and R.J. Turner, 1982. Wave-produced bubbles observed by side-scan sonar. Nature, vol. 296, 636-638.

Toba, Y., 1973. Local balance in the air-sea boundary processes, III. On the spectrum of wind waves. J. Oceanogr. Soc. Japan, vol. 29, 209-220.

U.S. Army Coastal Engineering Research Center, 1984. Shore protection manual: Vol. 1. U.S. Government Printing Office, Washington.

U.S. Department of the Navy, 1969. Physics of Sound in the Sea. U.S. Government Printing Office, Washington.

Weissman, M.A., S.S. Atakturk and K.B. Katsaros, 1984. Detection of breaking events in a wind-generated wave field. J. Phys. Oceanogr., vol. 14, 1608-1619.

Wu, J., 1981. Bubble populations and spectra in near-surface ocean: summary and review of field measurements. J. Geophys. Res., vol. 86, C1, 457-463.

VITA

Surname: Crawford Given Names: Gregory Blair

Place of Birth: Calgary, Alta. Date of Birth: January 11, 1960

Educational Institutes Attended:

University of Victoria, B.C. 1978-1985

Degrees Awarded:

B.Sc. (Honours Co-op) 1983 University of Victoria

Honours and Awards:

B.C. Provincial Scholarship (1978)

U.Vic. President's Entrance Scholarship (1978)

U.Vic. President's Scholarship (1979, 1981, 1982)

Frank and Margaret Gibbs Scholarship (1982)

N.S.E.R.C. Postgraduate Scholarship (1983, 1984)

B.C. G.R.E.A.T. Award (1983, 1984)

R.M. Pearce Memorial Scholarship (1984)

Publications:

Farmer, D.M. and G.B. Crawford, 1983. Measurements of acoustic correlation in the ocean with a high frequency echo-sounder. Nature, vol. 301, no. 5902, pp. 698-700

Lataitis, R.J., G. Crawford and S.F. Clifford, 1984. Sound scattering in a turbulent medium. J. Acoust. Soc. Amer., vol. 75, supplement 1, p. S-74.

PARTIAL COPYRIGHT LICENSE

I hereby grant the right to lend my thesis or dissertation (the title of which is shown below) to users of the University of Victoria Library, and to make single copies only for such users or in response to a request from the Library of any other university, or similar institution, on its behalf or for one of its users. I further agree that permission for extensive copying of this thesis for scholarly purposes may be granted by me or a member of the University designated by me. It is understood that copying or publication of this thesis for financial gain shall not be allowed without my written permission.

Title of Thesis/Dissertation:

Observations of the Spatial Distribution of Bubbles Generated By Breaking Waves

Author [redacted]

GREGORY BLAIR CRAWFORD

October 3, 1985